Per. Mineral. (2007), 76, 2-3, 267-308
SPECIAL ISSUE: In honour of Ezio Callegari on his retirement

doi:10.2451/2007PM0029
http://go.to/permin

PERIODICO di MINERALOGIA
established in 1930

An International Journal of
MINERALOGY, CRYSTALLOGRAPHY, GEOCHEMISTRY, ORE DEPOSITS, PETROLOGY, VOLCANOLOGY
and applied topics on *Environment*, *Archaeometry* and *Cultural Heritage*

P-T evolutions *vs.* numerical modelling: a key to unravel the Paleozoic to early-Mesozoic tectonic evolution of the Alpine area

Maria Iole Spalla[1 *] and Anna Maria Marotta[2]

[1] Dipartimento di Scienze della Terra "A. Desio", Sezione di Geologia dell'Università degli Studi di Milano and CNR-IDPA, Via Mangiagalli, 34, 20133 Milano, Italy.
[2] Dipartimento di Scienze della Terra "A. Desio", Sezione di Geofisica dell'Università degli Studi di MIlano, Via Cicognara, 7, 20129 Milano, Italy.

Abstract. — The pre-Alpine continental crust of the Alps preserves Permian-Triassic magmatic and high-temperature (HT) metamorphic evolutions, which overprinted records of Variscan subduction and collision-related metamorphism. The occurrence of numerous Variscan eclogites in the pre-Alpine continental crust, presently belonging to different structural domains, indicates that part of the Variscan suture zone occurs in the Alpine belt. The late Variscan evolution took place from 340 to 300 Ma, and therefore the igneous and metamorphic signatures up to Upper Carboniferous may represent the record of the late orogenic evolution. On the contrary, different authors interpreted the HT metamorphism associated with gabbro to granite intrusions younger than 290 Ma as the effect of Permian-Triassic late-orogenic collapse or continental rifting. The goal of this study is to reduce the ambiguity about the geodynamic significance of the Permian-Triassic HT metamorphism and igneous activity in the Alpine continental crust, with the support of numerical modelling of: ocean subduction, continental collision, lithospheric detachment and subsequent gravitational thermal relaxation. Comparison of the model predictions with structural and petrologic data has driven the successive model refinements to improve the fit. The best fit model predictions show a rather good agreement with natural data (coincidence of age, P-T values and rock compositional affinity) up to late-Variscan times. The poor agreement during the Permian-Triassic evolution suggests that, with respect to the thermal state established during the post-collisional gravitational evolution, an additional positive heat anomaly is necessary to induce the thermal state indicated by natural P-T estimates.

Riassunto. — La crosta continentale pre-Alpina delle Alpi preserva impronte metamorfiche di alta temperatura e magmatiche di età Permo-Triassica che si sovrappongono a quelle registrate durante la subduzione e collisione Varisiche. La ricorrenza di numerose eclogiti Varisiche nella crosta continentale pre-Alpina, che attualmente costituisce differenti domini strutturali delle Alpi, indica che parte della zona di sutura Varisica è attualmente preservata nella catena alpina. L'evoluzione tardo-Varisica si compie tra 340 e 300 Ma, e quindi le impronte ignee e metamorfiche che si sono registrate entro il Carbonifero superiore sono i segnali dell'evoluzione tardo-orogenica. Al contrario, il metamorfismo di alta temperatura associato con l'intrusione di gabbri e di graniti più giovane di 290 Ma è stato interpretato da vari autori come l'effetto di un collasso tardo-orogenico o di un rifting continentale Permo-Triassici. Lo scopo di questo studio è di ridurre l'ambiguità sul significato

* Corresponding author, E-mail: iole.spalla@unimi.it,

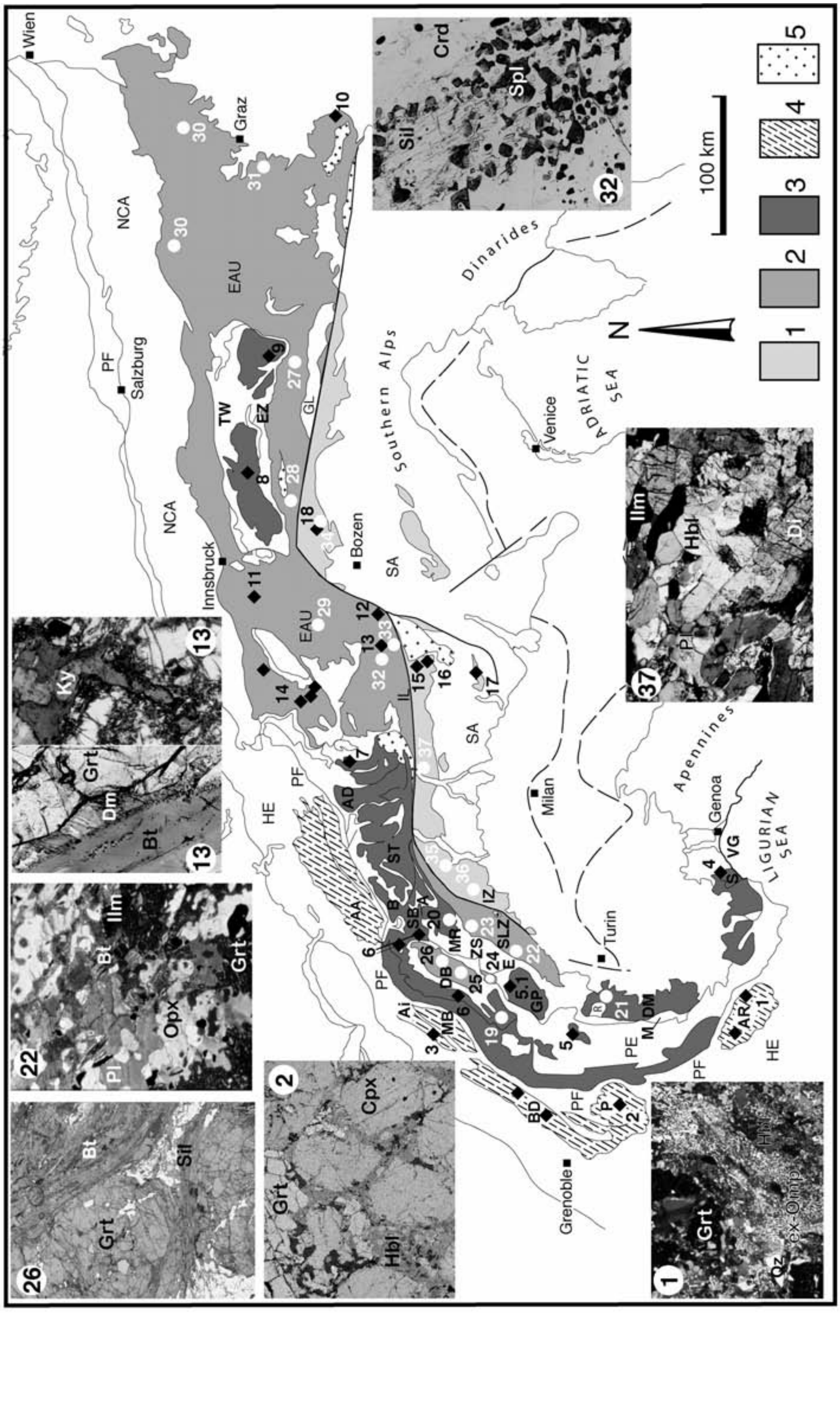
Wien
Graz
Salzburg
Innsbruck
Bozen
Venice
Milan
Turin
Genoa
Grenoble
NCA
EAU
PF
TW
EZ
GL
SA
HE
IL
IZ
SLZ
Southern Alps
Dinarides
Apennines
ADRIATIC SEA
LIGURIAN SEA
N
100 km
1
2
3
4
5

geodinamico del metamorfismo di alta temperatura e dell'attività ignea Permo-Triassici che caratterizzano la crosta continentale alpina con l'ausilio della modellizzazione numerica di: subduzione oceanica, collisione continentale, distacco litosferico e successivo rilassamento termico gravitazionale. Il confronto delle previsioni dei modelli con i dati strutturali e petrologici ha guidato i raffinamenti dei modelli successivi, mirati a migliorare l'accordo tra previsioni e dati naturali. Il modello caratterizzato dalla migliore aderenza delle previsioni ai casi naturali (in termini di coincidenza di età, valori P-T e affinità composizionale delle rocce) mostra una buona corrispondenza fino all'evoluzione tardo-Varisica. Lo scarso accordo durante l'evoluzione Permo-Triassica suggerisce che sia necessaria un'anomalia termica positiva addizionale per indurre lo stato termico adatto a soddisfare le condizioni P-T stimate nelle rocce naturali, rispetto a quello che si instaura durante l'evoluzione post-collisionale gravitativa.

Key Words: *HT Permian-Triassic metamorphism, Variscan convergence, numerical modelling*

Introduction

High thermal regimes in the continental lithosphere can be induced, for instance, either by thickening consequent to continental collision, or by astenospheric upwelling related to lithospheric thinning (e.g. Thompson, 1981; England and Thompson, 1984; Thompson and England, 1984; Sandiford and Powell, 1986; Peacock, 1989; Beardsmore and Cull, 2001). The individuation of the geodynamic scenario responsible for high thermal regime setting is not univocal, especially in a continental lithosphere, which has been repeatedly forged in active margins. This is the case of the Alps, where post-Variscan igneous and metamorphic records of a Permian-Triassic high thermal regime are detectable along the whole belt, from the Ligurian sea to the Pannonian Basin, even in domains strongly reworked by the Alpine tectonics and metamorphism (Fig. 1), as those actually constituting the axial part of the orogen. These records consist of a widespread emplacement of Permian-Triassic basic to intermediate intrusive stocks, associated with regional high temperature - low pressure (HT-LP) metamorphism, which postdates the structures and metamorphic imprints developed during Variscan subduction and collision. The main feature in the pre-Alpine continental crust of the different structural domains (Helvetic, Penninic, Austroalpine and Southalpine) is the occurrence of eclogites: the exposure of Variscan rocks within the present-day Alpine structural domains indicates that part of the Variscan suture zone has been recycled in the Alpine belt construction.

If the structural, igneous and metamorphic imprints of the late Variscan evolution (from 340 to 300 Ma) are widely recorded all along

Fig. 1 (previous page) – Tectonic map of the Alps with the location of Variscan (black diamonds) and Permian-Triassic (white dots) metamorphic rocks occurring in the pre-Alpine continental crust. Labels are as in Tables 1 and 2 and in Figs. 3 and 4. Labels of the photomicrographs correspond to the sample location on the tectonic map. 1: re-equilibrated eclogite from the Malinvern-Argentera Complex of the Argentera Massif, Helvetic Domain. The eclogitic assemblage of Grt, Omp, Hbl I, Qz and Rt is replaced by Di, Pl, Hbl II and Ilm. A fine-grained symplectite of Di and Pl overgrows Omp (ex-Omp). Crossed polarisers, long side of the photomicrograph ≈5.5 mm. 2: BSE-SEM image of eclogite from the Pelvoux Massif (di Paola, 2001). Cpx and Grt are rimmed by new Hbl and Pl. Long side of the BSE image is 1.5 mm. 13 left: HP–HT gneiss from the Languard-Campo Nappe, Austroalpine Domain of Central Alps. Relic of partially replaced dumortierite (Dm) is preserved in a Grt-Bt gneiss. Plane polarized light, long side of the photomicrograph ≈ 4 mm; 13 right: Ky relics, rimmed by Qz, are preserved in Crd-bearing gneiss. Crossed polarisers, long side of the photomicrograph ≈5 mm. 32: Crd-Spl-Sil- bearing acid granulite from the Sondalo Gabbro country rocks, Austroalpine Domain of Central Alps. Plane polarized light, long side of the photomicrograph ≈6 mm. 37: Di-bearing amphibolite from the Dervio-Olgiasca Zone, Southalpine Domain. The foliation marked by Hbl SPO is synchronous with 226 ± 2 Ma pegmatite emplacement. Crossed polarisers, long side of the photomicrograph ≈3 mm. Mineral abbreviations as in (Kretz, 1983). Legend: 1) Southalpine basement, 2) Austroalpine basement, 3) Penninic basement, 4) Helvetic basement, 5) Tertiary intrusive stocks; EAU: Eastern Austroalpine, HE: Helvetic, NCA: Northern Calcareous Alps, PE: Penninic, SA: Southalpine; A: Antrona Zone, AA: Aar Massif, AD: Adula Nappe, Ai: Aiguilles Rouges Massif, AR: Argentera Massif, B: Berisal Complex, BD: Belledonne Massif, DB: Dent Blanche Klippe, DM: Dora Maira Massif, E: Mt. Emilius Klippe, EZ: Tauern Eclogite Zone, G: Gotthard Massif, GL: Gailtal Line, GP: Gran Paradiso Massif, IL: Insubric Line, PF: Penninic Front, IZ: Ivrea Zone, M: Monviso Complex, MB: Mont Blanc Massif, MR: Monte Rosa Nappe, P: Pelvoux Massif, R: Rocciavrè Complex, S: Savona Nappe, SB: St Bernard Nappe, ST: Simplon-Ticino Nappes, SLZ: Sesia-Lanzo Zone, TW: Tauern Window, VG: Voltri Group, ZS: Zermatt-Saas Zone.

the European Variscan belt, the imprints of the Permian-Triassic high thermal regime, such as the HT-LP metamorphism associated with gabbro to granite intrusions, are peculiar of the Alpine belt. The overprint of HT Permian-Triassic evolution on the relics of the Variscan orogeny makes the interpretation of the anomalously-high thermal regime ambiguous. In fact, it can be interpreted as induced by either a late-orogenic collapse or lithospheric extension and thinning leading to continental rifting. In both cases the Permian-Mesozoic rifting has to be engaged within a continental lithosphere, which has been previously thermally softened and thinned by the lithospheric unrooting during mature collision.

We attempt to solve the dualistic interpretation on the geodynamic significance of the Permian-Triassic HT-LP metamorphism and igneous activity with the support of a numerical model. The goal is to compare the modeling predictions with the P-T climax conditions of Variscan and Permian-Triassic metamorphism affecting the continental crust of the Alpine structural domains, from the external to the internal chain. At this purpose we have implemented successive finite element schemes to model ocean subduction leading to continental collision, lithospheric detachment and subsequent gravitational thermal relaxation of the system. The predictions from each model have been compared with natural data and the results of the comparison have driven the successive model refinement to improve the fit of natural data with model predictions.

Geologic Outline

Superposed structural and metamorphic imprints affected the rocks forming the Alpine nappe belt, during successive convergent and divergent tectonic regimes. However, in spite of the deep subduction of a large amount of continental lithosphere, from both facing continental margins, during Alpine times, relict metamorphic and igneous imprints recorded during the Variscan convergence and the successive Pangea break-up survived in the pre-Alpine continental crust.

Nappes in the Alps have been attributed to the different structural domains (Fig. 1) on the basis of their location in the present-day structural position, which is generally considered as a consequence of their commonly accepted paleogeography. The lithostratigraphic setting and the tectonic style have been initially the discriminating factors in individuating the subdivision in nappe systems. Such an approach was later on implemented by the metamorphic history (Spalla *et al.*, 1996 and refs. therein). The main structural domains (Fig. 1) recognizable along a cross section, from the external to the internal part of the chain, are (e.g. Polino *et al.*, 1990; Dal Piaz *et al.*, 1993; Pfiffner *et al.*, 1997; Schmid *et al.*, 2004):

1. the European Foreland, flexured and thrusted underneath the Alpine orogeny at the lithosphere scale, during final stages of plate convergence;
2. the Helvetic domain, with a basement mainly characterised by pre-Alpine structural, metamorphic and stratigraphic signatures. Since the Palaeogene continental collision, Alpine tectonics reactivated the Mesozoic listric normal faults of the European passive margin into a thick-skin thrust system of basement and cover slices;
3. the Penninic and Austroalpine heterogeneous nappe system, constituting the axial part of the belt, deformed and metamorphosed since Cretaceous, during oceanic subduction, exhumation and continental collision. It forms a mélange of thin continental and oceanic basement and cover nappes, the last ones belonging to the sutured Tethys ocean;
4. the Southalpine domain structured as a South-verging thrust system of continental basement and cover units since Cretaceous (e.g. Brack, 1981; Milano *et al.*, 1988) and locally displaying a weak Alpine metamorphic imprint. It constitutes the hinterland of the early-Alpine belt.

This tectonic framework has been constrained and synthesised in lithospheric images by the ECORS-CROP-NFP20-TRANSALP project (e.g. Cassinis, 2006 and refs. therein). In the seismic profiles the Cretaceous to Palaeogene rootless crustal prism in the axial part of the chain is recognisable, limited by the Penninic Front (PF in Fig. 1) towards the Helvetic Domain (European Plate) and by the Periadriatic Lineament (IL and GL in Fig. 1) towards the Southalpine Domain (Adria Plate) (e.g. Platt, 1986; Platt, 1993; Polino *et al.*, 1990; Spalla *et al.*, 1996; Dal Piaz *et al.*, 2001). This rootless crustal prism is underthrusted by exotic Moho, or continental crust, either from the northern or the southern plates and bounded laterally by recently active tectonic structures. All the Alpine high to ultra-high pressure rocks formed in the Cretaceous to Late-Eocene time span and are located in this part of the chain, as pointed out by a recent compilation of radiometric data at the scale of the belt (Handy and Oberhaensli, 2004 and refs. therein). This idea envisages Alpine eclogite formation in rocks of continental origin, both through continental collision or pre-collision models. In the latter case subduction of the European oceanic lithosphere (lower plate), carrying possibly a number of micro-continents or small mantle-free crustal fragments, thickened the overriding crust by underplating. Alternately, the high-pressure continental units, forming the orogenic wedge, were derived from the active margin through tectonic erosion of its continental toe, before the continental collision onset (e.g. Platt, 1986; Polino *et al.*, 1990; Spalla *et al.*, 1996; Dal Piaz *et al.*, 2001).

Variscan to Permian-Triassic Evolution

Pre-Alpine rocks are well preserved in the Helvetic domain, in which they are poorly re-equilibrated during Alpine recrystallisation, and in the Southalpine domain, where the exposed sections almost completely escaped the Alpine metamorphism. Relics of the convergent and divergent pre-Alpine evolution are preserved also in the Penninic and Austroalpine nappe system, even if here the pervasive Alpine structural and metamorphic reworking makes them more scattered. Pods of pre-Alpine metamorphic and igneous rocks occur within several Alpine basement units, where the eclogitic, granulitic, migmatitic and amphibolitic records of Variscan subduction and collision are widespread (Fig. 1 and insets 1, 2 and 13) and well constrained in time and metamorphic P-T evolution (Fig. 2, Table 1) (e.g. Dal Piaz *et al.*, 1993; Colombo and Tunesi, 1999; Desmons *et al.*, 1999; Neubauer *et al.*, 1999; von Raumer *et al.*, 1999). Pre-Alpine metaophiolite remnants in Helvetic to Austroalpine domains (e.g. Miller and Thoeni, 1995; Guillot *et al.*, 1998; Nussbaum *et al.*, 1998) highlight that parts of the Variscan suture zone were incorporated in the Alpine belt, and that oceanic lithosphere subduction and related low thermal regime were effective during the accretion of pre-Alpine continental crust at a convergent plate margins.

Models explaining the evolution of the Variscan convergence have generally been derived from Central European chains (i.e. French Massif Central, Bohemian Massif; Tait *et al.*, 1997; Torsvik, 1998; Faure *et al.*, 2004) and papers taking into account the evolution of the Palaeozoic lithosphere of the Alps in the plate motion reconstruction at wider scale are rare (von Raumer and Neubauer, 1993; von Raumer *et al.*, 2002; von Raumer *et al.*, 2003). Palaeomagnetic data suggest that the European Variscan belt formed during Palaeozoic collision between Gondwana (to the South) and Laurentia and Baltica (to the North) continents, trapping some minor plates (simply Avalonia and Armorica or a more complex configuration envisaging the occurrence of Hunich terranes). Palaeogeographic plates configuration, subduction vergence and number of involved oceans (e.g. Rheic, Moldanubicum Central Massif and PalaeoTethys) are still under discussion (Oliver *et al.*, 1993; Finger and Quadt, 1995; Tait *et al.*, 1997; Torsvik, 1998; von Raumer *et al.*, 2002; von Raumer *et al.*, 2003); however, the interpretation of the evolution of the European Palaeozoic chain is founded on two types of models: monocyclic (e.g. Bard *et al.*, 1980; Matte, 1986; Ledru *et al.*, 1989) and polycyclic (e.g. Pin and Peucat, 1986; Ziegler, 1986; Pin, 1990; Boutin *et al.*, 1995; Faure *et al.*, 1997). In the monocyclic models the evolution can be subdivided in three main orogenic periods (Ledru *et al.*, 1989): the early-Variscan (≥ 400 Ma), coinciding with a oceanic and continental crust subduction stage; the meso-Variscan (400-340 Ma), interpreted as the continental collision stage; the neo-Variscan (350-280 Ma), characterised by the development of strike-slip tectonics and granitoids emplacement between 350 and 320 Ma (Matte, 1986; Malavieille *et al.*, 1990; Malavieille, 1993), and followed by the opening of Upper Carboniferous basins.

Some common characters can be recognized among different models: the occurrence of a ≈2500 km wide ocean, between the Avalonia-Armorica plates and the Alpine Paleozoic terranes (belonging to Gondwana or to Hunic terranes); an active subduction between 425 and 380-370 Ma, followed by continental collision and late orogenic

Table 1
Assemblages and physical conditions of Variscan metamorphism recorded in the crustal and mantle rocks of the Alps.

tectonic system	key	location	assemblages	lithologies	T(K)	P(GPa)	age (Ma)	method	refs.
HD (Ar)	1a	Tinèe	Grt + Hbl + Cpx + Plg + Qtz	metabasics	983-1033	1.2-1.4	428-420	(U/Pb)	(1)
HD (Ar)	1b	Malinvern-Argentera	Grt + Hbl + Cpx + Plg + Qtz + Rt/Ilm	eclogitic gneisses	1053-1103	1.5-1.8	352-326	(U/Pb)	(2; 3; 4; 5)
HD (Bd)	2	Rocher Blanc Lac la Croix Beaufortin	Grt + Cpx + Plg + Qtz + Rt + Zr Grt + Hbl + Cpx + Qtz + Rt + Zo	metabasics	913-973	1.1-1.3	403-387	(U/Pb)	(6; 7; 8)
HD (Pe)	2	Oisan	Cpx+Grt+Qtz+Rt	metabasics	-	-	Variscan (425-295)		(9)
HD (Ai)	3	Lac Cornu	Grt + Cpx + Hbl + Qtz + Rt	metabasics	1053	≥ 1.1	403-387	(U/Pb)	(10; 7; 11)
PN (SM)	4	Savona	Grt+Omp+Qtz+Phe	metabasics	873-913	> 1.2	425-395	(Sm/Nd U/Pb)	(12; 7)
PN (Ab)	5	Cottian Alps	Grt + Ms + Pl + Ky + Rt + Qtz	metapelites	823-923	0.8-1.1	360-340	(Ar/Ar)	(13; 14)
PN (GP)	5.1	Gran Paradiso	Grt + St + Ilm + Qtz	metapelites	713-893	0.5-0.6	Variscan (425-295)		(15)
PN (Bd)	6a	Ruitor	Grt + Bt + Sil/And	metapelites	823 - 873	0.5-0.8	328-332	(U/Pb)	(16; 17)
PN (Bd)	6b	Siviez-Mischabel	Hbl + Plg + Qtz	metabasics	833-923	>1.5	Variscan (425-295)		(18; 19)
PN (Su)	7	Suretta	Grt + Hbl ± Cpx + Ep + Qtz	metabasics	898-1023	≥ 2.0	pre-Alpine (Variscan?) (425-295)		(20)
PN (IS)	8	Frosnitztal	Grt+Omp+Qtz	metabasics	673-773	0.8-1.2	400-437	(Sm-Nd; U/Pb)	(21; 22)
PN (IS)	9	Doesenertal	Grt+Omp+Qtz	metabasics	793-993	> 1.2	400-437	(Sm-Nd; U/Pb)	(23; 22)
AU (TZ)	10a	Pohorje	Grt-bearing ultramafics	ultramafics, metabasics	1023-1143	3.0-3.6	Variscan(?) (425-295)		(24; 25; 26)
AU (TZ)	10b	Pohorje	Grt + Omp + Qtz ± Ky	metabasics	903-973	1.8-2.5	Alpine(?) Variscan(?) (425-295)		(27)

AU (Oe)	11	Central Oetztal	Grt+Omp	metabasics	973-1073	2.5-2.9	370-340	(Sm-Nd; Rb-Sr)	(28; 29)
AU (TZ)	12a	Ultental	Grt + Bt + Pl + Kfs + Ky + Rt	metapelites	913-973	1.0-2.0	365	Pb/Pb	(30; 31)
AU (TZ)	12b	Ultental	Grt+Omp+Qtz	metabasics	923-1023	1,2-1,6	360	Ar/Ar	(31)
AU (TZ)	12c	Ultental	Grt-bearing ultramafics	ultramafics	1043-1083	2.2-2.8	334-326	Sm/Nd	(32; 33; 34)
AU (LCN)	13a	Mortirolo	Dum+Qtz	metapelites	˜1073	>2.0	early-Variscan (425-375)		(35)
AU (LCN)	13b	Mortirolo	Di + Grt ± Scp + Pl + Qtz	metabasics	1023-1223	0.65-0.9	>314 (370-314)		(36)
AU (Sil)	14a	SE Silvretta	Grt + Hbl ± Cpx + Plg + Qtz	metabasics	873-953	0.55-0.75	353-387	Rb/Sr	(37; 38)
AU (Sil)	14b	Silvretta (Pischahorn)	Qtz + Ms + And	metapelites	˜873	˜0.2	353≥ t ≥280 (353-295)	Rb/Sr K/Ar	(39)
AU (Sil)	14c	Silvretta (Val Puntona)	Grt + Omp + Qtz + Rt ± Phe	metabasics	673-723	2.5-2.7	early-Variscan (425-375)		(40)
AU (Sil)	14d	Silvretta (Ischgl)	Grt + Omp + Qtz + Rt ± Phe	metabasics	723-773	2.3-2.9	early-Variscan (425-375)		(40)
SA	15	Valtellina	Grt + St + Bt + Ms + Plg + Qtz	metapelites	843-933	0.85-1.15	˜330		(41)
SA	16	Val Camonica	Grt + St + Bt + Ms + Plg + Qtz	metapelites	843-893	1.0-1.2	˜330		(42)
SA	17	Val Trompia	Grt ± Cld+ Bt + Ms + Plg + Qtz	metapelites	773-823	0.9-1.3	349-379	(Rb-Sr)	(43; 44; 45; 46)
SA	18	Eisacktal	Crd + Sil + Bt	metapelites	˜923	˜0.2	˜350		(47)

Absolute age estimates are expressed as age intervals which represent the minimum and maximum values of the error bar (the dating method is specified in the column Method). The age indication based on geological constrains is expressed in brackets and the column Method is empty. Key as in Fig. 1 and $P_{max}T_{Pmax}$ values are represented in Fig. 2; HD: Helvetic Domain, PN: Penninic Domain, AU: Austroalpine Domain, SA: Southalpine Domain, Ab: Ambin, Ar: Argentera, Bb: Briançonnais basement, Bd: Belledonne, Ai: Aiguilles Rouges, GP: Gran Paradiso, Oe: Oetztal, Pe: Pelvoux, Sil: Silvretta, SM: Savona Massif, TZ: Tonale Zone. Reference key: 1= Latouche and Bogdanoff, 1987; 2= Menot and Paquette, 1993; 3= Colombo *et al.*, 1994; 4= Lombardo *et al.*, 1997; 5= Rubatto *et al.*, 2001; 6= Vivier *et al.*, 1987; 7= Paquette *et al.*, 1989; 8= Guillot *et al.*, 1998; 9= di Paola, 2001; 10= Ligeois and Duchesne, 1981; 11= von Raumer *et al.*, 1999; 12= Messiga *et al.*, 1992; 13= Borghi *et al.*, 1999; 14= Moniè, 1990; 15= Le Bayon *et al.*, 2006; 16= Bussy *et al.*, 1996; 17= Giorgis *et al.*, 1999; 18= Thélin *et al.*, 1990; 19= Thélin *et al.*, 1993; 20= Nussbaum *et al.*, 1998 and refs. therein; 21= Zimmermann and Franz, 1989; 22= von Quadt *et al.*, 1997; 23= Droop, 1983; 24= Hinterlechner *et al.*, 1991a; 25= Hinterlechner *et al.*, 1991b; 26= Janak *et al.*, 2003; 27= Sassi *et al.*, 2004; 28= Miller and Thoeni, 1995; 29= Konzett *et al.*, 2005; 30= Hauzenbeger *et al.*, 1993; 31= Godard *et al.*, 1996; 32= Herzberg *et al.*, 1977; 33= Tumiati *et al.*, 2003; 34= Morten *et al.*, 2004 and refs. therein; 35= Gosso *et al.*, 1995; 36= Zucali, 2001; 37= Maggetti and Galetti, 1988; 38= Melcher *et al.*, 2002; 39= Brugger, 1994; 40= Schweinehage and Massonne, 1999; 41= Spalla *et al.*, 1999 and ref. therein; 42= Spalla *et al.*, 2006; 43= Del Moro in Riklin, 1983; 44= Giobbi and Gregnanin, 1983; 45= Spalla *et al.*, 2004; 46= Spalla *et al.*, 2007; 47= Benciolini *et al.*, 2006.

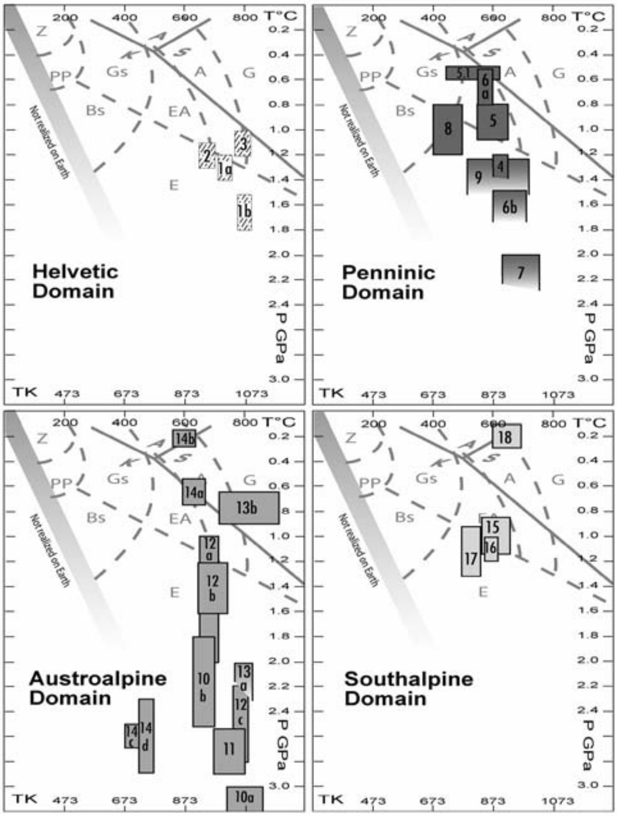

Fig. 2 – P-T estimates of the baric peak of Variscan metamorphic rocks occurring in the Helvetic, Penninic, Austroalpine and Southalpine Domains. Patterns of P-T boxes correspond to the tectonic domains of Fig. 1. Ages, P-T estimates and references are reported in Table 1. Keys are as in Fig. 1 and Table 1. The petrogenetic grid showing the metamorphic facies fields as reference is redrawn after Spear (1993) and Al_2SiO_5 triple point after Holdaway (1971); Z: zeolite facies, PP: prehnite-pumpellyite facies, Gs: greenschist facies, Bs: blueschist facies, E: eclogite facies, EA: epidote-amphibolite facies, A: amphibolite facies, G: granulite facies, *A*: andalusite, *S*: sillimanite, *K*: kyanite.

collapse (Pin and Peucat, 1986; Ledru *et al.*, 1989; Malavieille, 1993; Tait *et al.*, 1997; Torsvik, 1998; von Raumer *et al.*, 2003; Faure *et al.*, 2004).

In this scenario, the Permian high thermal regime affecting the Alpine continental lithosphere has been interpreted as an effect of the late-orogenic collapse of the Variscan belt, enhanced by the lithospheric unrooting (Malavieille *et al.*, 1990; Ledru *et al.*, 2001), or as the consequence of lithospheric thinning, leading to continental rifting, as already proposed for the Austroalpine and Southalpine domains (Lardeaux and Spalla, 1991; Diella *et al.*, 1992; Dal Piaz, 1993; Schuster *et al.*, 2001). The second interpretation appears more suitable if the Carboniferous/Permian transition of the Palaeozoic plate convergence into a transtensional to extensional tectonic regime, announcing the Pangea break-up (e.g. Golonka *et al.*, 1994), is considered. Pull-apart basins testify the thinning of thickened Variscan crust during this period (Wopfner, 1984; Ziegler, 1993) and predate the marine transgression from the East, where the Neotethys Ocean is opening (Muttoni *et al.*, 2003). The Permian-Triassic igneous activity and the associated metamorphism indicate a P/T ratio compatible with extensional tectonics related to astenosphere upwelling. The distribution of magmatic and metamorphic products has been used to interpret the rifting as asymmetric, with Austroalpine and Southalpine basement constituting the hanging-wall (e.g. Lardeaux and Spalla, 1991; Diella *et al.*, 1992; Quick *et al.*, 1992; Dal Piaz, 1993) and where the new divergent regime gradually evolved up to the Upper Jurassic formation of the Western Tethys oceanic lithosphere.

Variscan to Permian-Triassic Metamorphic Record

Variscan - The Variscan syn-metamorphic tectonics is well recorded in the continental crust of Helvetic to Austroalpine domains. In the P-T quantitative data review here synthesised (Table 1 and Fig. 2) data exclusively related to P_{max} imprints have been selected because they are the most representative to indicate the thermal state at maximal pressures recorded during the subduction-collision tectonic cycle. The time constraints associated to the P-T values are based on radiometric and field data as described in the literature. In the *Helvetic Domain* eclogite facies rocks (insets 1 and 2 of Fig. 1), granulites, amphibolites, high-grade metasediments and metagranitoids (Figs. 1, 2 and Table 1) testify the Variscan convergence (e.g. Paquette *et al.*, 1989) and have been described in the Argentera, Pelvoux-Belledonne, Aiguilles Rouges and Mt. Blanc massifs (von Raumer, 1974; Liegeois and Duchesne, 1981; Latouche and Bogdanoff, 1987; Bogdanoff *et al.*, 1991; von Raumer *et al.*, 1999). Eclogites and related high-pressure rocks are preserved in core pods, wrapped by high-grade foliations in migmatitic gneisses and characterised by a rim widely re-equilibrated under amphibolite or granulite facies conditions. Migmatitic foliation and high-pressure boudins are intersected by Late Palaeozoic igneous rocks. A few relics of eclogites and high-pressure rocks are yet preserved as discrete pods within mafic lenses of the *Penninic* poly-metamorphic basement of Savona Massif (Messiga *et al.*, 1992), of Siviez-Mischabel complex (Thelin *et al.*, 1990; Rahn, 1991; Thelin *et al.*, 1993), and of the SE Tauern window (Droop, 1983; Zimmerman and Franz, 1989; Droop *et al.*, 1990). The dominant metamorphic imprint of continental protoliths is mainly recorded under epidote-amphibolite- or amphibolite-facies conditions (Figs. 1, 2 and Table 1), which are peculiar of the base of a stable continental crust or of continental collision settings. The Variscan ages have been supported by numerous radiometric data (e.g. Monié, 1990; Bussy *et al.*, 1996; von Quadt *et al.*, 1997). High-pressure rocks of the Eastern *Austroalpine* basement nappes are located around the Tauern window, in the Oetztal, Silvretta and Languard-Campo nappes (inset 13 of Fig. 1) and at the South-Eastern end of the Austroalpine domain (Fig. 1). Here eclogites and associated ultramafic rocks from Pohorje massifs occur as pods, up to kilometre scale, within poly-metamorphic paragneisses, often associated to kyanite-bearing schists and mylonites, with minor relict metagabbros, marbles and manganiferous cherts. Protoliths of eclogites are Cambrian to early Ordovician, low-Ti cumulus gabbros and Fe-Ti MORB (e.g Gebauer and Soellner, 1993; Miller and Thoeni, 1995). Variscan eclogites and related rocks occur also in Ulten and Silvretta basement (e.g. Godard *et al.*, 1996; Morten *et al.*, 2004). These pods are locally preserved within large bodies mainly derived from gabbros and related ultramafic cumulates and predate the amphibolite-facies regional imprint. The eclogitic ultramafics from the Ulten complex are associated with bodies of spinel-lherzolite evolving to fine-grained garnet peridotite (e.g. Herzberg *et al.*, 1977; Morten *et al.*, 2004); this association suggests cooling within a deep subduction environment. Some Silvretta eclogites, deriving from MORB protoliths, have early-Variscan ages (Schweinehage and Massonne, 1999). HP Variscan rocks (Fig. 2 and Table 1) derive not only from mantle or oceanic crust protoliths but also from continental crust (e.g. Hauzenberger *et al.*, 1993; Gosso *et al.*, 1995), testifying the deep involvement of continent slices in the subduction zone during the still active oceanic subduction, or the early stages of the continental collision. In the *Southalpine Domain*, metamorphic Variscan ages are mainly meso-Variscan, and ages of 330-340 Ma have been interpreted as dating the amphibolite-facies thermal peak (e.g. Boriani and Villa, 1997; Spalla and Gosso, 1999; Benciolini *et al.*, 2006). This Variscan basement mainly consists of metapelites, amphibolites, metagranitoids, quartzites, carbonatic schists, marbles and pegmatites. Well-constrained metamorphic evolutions, integrating structural and petrologic investigations, have been performed mainly on metapelites (Fig. 2, Table 1) in which re-equilibrations under low-temperature – intermediate-pressure (LT-IP) conditions, recorded during the Variscan P-T prograde path and predating the P-climax, are preserved where the dominant fabric at the regional scale is a penetrative foliation marked by amphibolite-facies minerals (Spalla *et al.*, 1999).

Permian-Triassic - The Permian-Triassic HT-LP metamorphism is associated with mafic to acidic igneous activity, testified by gabbro and diorite stocks (Tables 2 and 3, Figs. 1, 3 and 4), frequently associated with sub-continental peridotites, and occurring in the axial part of the belt and in the Southalpine hinterland (e.g. Brodie *et al.*, 1989; Bonin *et al.*, 1993; Rottura *et al.*, 1998; Schuster *et al.*, 2001; Sthaele *et al.*, 2001b; Rampone, 2002; Spalla and Gosso, 2003), but does not affect the *Helvetic Domain*. P-T evolutions have no peculiar character in the singular structural domains, as it is the case for the lithostratigraphy of tectonic units recording the HT Permian-Triassic imprints. Metamorphic evidences of Permian-Triassic lithospheric thinning have been widely described in lower, intermediate and upper continental crust of Austroalpine and Southalpine Domains, but only a few records are recognized in the upper and intermediate Penninic crust of Western Alps (Figs. 1 and 3, Table 2). In the data review of Table 2 and Fig. 3, we selected the P-T estimates related to T_{max} imprints, which better highlight the thermal anomalies that can be generated by mantle up-welling during lithospheric thinning. In the *Penninic Domain*, HT assemblages occur in sillimanite-bearing metapelites and in metaintrusives. The pre-Alpine exhumation can occur following a P-retrograde path characterised by cooling (Bouffette, 1993) or by heating (Desmons, 1992). The high temperature metamorphism in the *Austroalpine Domain* is mainly recorded in sillimanite and biotite-bearing metapelites (inset 26 of Fig. 1), with associated minor mafic granulites

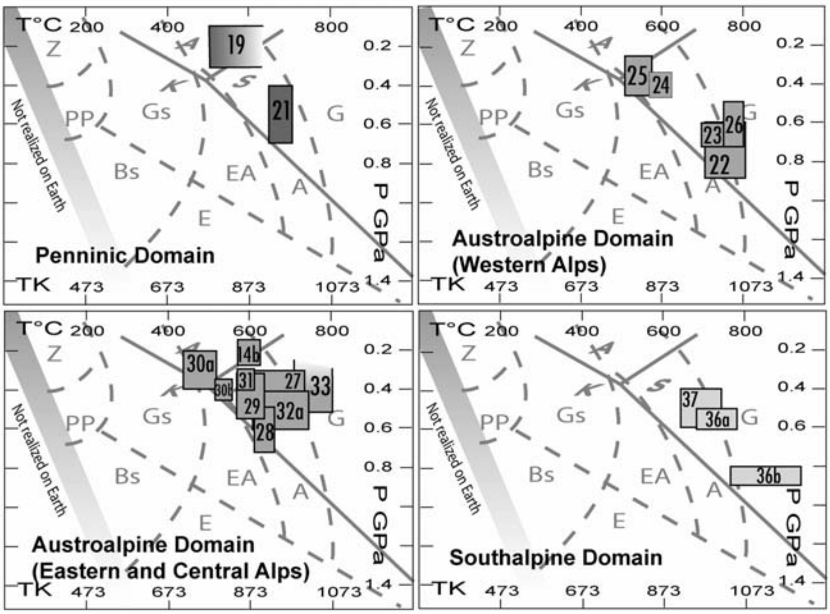

Fig. 3 – P-T estimates of the thermal peak of Permian-Triassic metamorphic rocks in Penninic, Austroalpine (Western Alps and Eastern-Central Alps) and Southalpine Domains. Patterns of P-T boxes correspond to the tectonic domains of Fig. 1. Ages, P-T estimates and references are reported in Table 2. Keys are as in Fig. 1 and Table 2. The petrogenetic grid showing the metamorphic facies fields as reference is redrawn after Spear (1993) and the Al_2SiO_5 triple point after Holdaway (1971). Legend as in Fig. 2.

(orthopyroxene- and garnet-bearing: inset 22 of Fig. 1), amphibolites, and high-grade marbles. Locally, a very HT metamorphic aureole developed in gabbro country rocks (#32b in Table 2, inset 32 of Fig. 1). Exhumation path may be characterized by cooling (e.g. Dal Piaz *et al.*, 1983; Stoeckhert, 1987; Vuichard, 1987; Lardeaux and Spalla, 1991), adiabatic decompression (e.g. Spalla *et al.*, 1995; Zucali, 2001) or by heating (e.g. Schuster *et al.*, 2001). In each case, large parts of the exhumation paths were accomplished under high thermal regime. Extension-activated exhumation of deep seated continental crust occurred up to shallow crustal levels, suggesting that some Austroalpine units belonged to a thinned continental margin, later subducted during Cretaceous convergence (e.g. Rebay and Spalla, 2001).

In the *Southalpine basement* Permian-Triassic HT metamorphism developed in metapelites, mafic granulites, amphibolites (inset 37 of Fig. 1) and high-grade marbles. In places contact aureole developed in country rocks where intrusions occur at shallow levels (#34 in Table 2). Exhumation was characterized by decompressional cooling (e.g. Brodie *et al.*, 1989) or by increasing temperature during decompression (e.g. di Paola and Spalla, 2000). Generally the exhumation paths are characterised by high T/P ratio.

Variscan to Permian-Triassic Magmatic Record

Variscan - The syn-collisional Variscan igneous activity in the pre-Alpine continental crust consists of peraluminous magmatic products derived from crustal melting and associated with high-K basic magmas (Bonin *et al.*, 1993). Lower to Middle Carboniferous high-K calc-alkaline suites indicate that partial melting occurred during decompression, which is accompanied by short-living strike-slip dominated tectonics. The oldest Carboniferous intrusives, widely diffused in the Helvetic Domain, have ages between 340 and 330 Ma, high Mg-number and sub-alkaline character with calc-alkaline to alkaline affinities (Debon and Lemmet, 1999). Late Carboniferous and Early Permian igneous activity took place at the end of the orogenic cycle associated with extensional tectonics. The igneous products have both alkaline and calc-alkaline characters (Bonin *et al.*, 1993). The Helvetic Mg-Fe or Fe plutonic rocks (low Mg-number) belong to this group and have radiometric ages comprised between 305 and 295 Ma (Debon and Lemmet, 1999).

Permian-Triassic – Together with the Permian-Triassic HT-LP metamorphism a widespread igneous activity with underplating of huge gabbro bodies (Fig. 4 and Table 3), frequently associated with sub-continental peridotites, is recurrent both in the axial belt and in the Southalpine hinterland (e.g. Brodie *et al.*, 1989; Bonin *et al.*, 1993; Schuster *et al.*, 2001; Sthaele *et al.*, 2001a; Rampone, 2002; Spalla and Gosso, 2003). In Southern Alps, Permian magmatism is testified by a continuum spectrum of rocks varying from basaltic andesites to rhyolites and from gabbros to monzogranites, emplaced in a time interval between 290 and 260 Ma (Rottura *et al.*, 1998). The occurrence of huge gabbro bodies is a peculiar character of the Alpine continental crust with respect to the rest of the European Variscan chain. Opposite to metamorphic and igneous records of the Variscan cycle (425-295 Ma), which occur from Helvetic to Southalpine, the Permian-Triassic magmatism and metamorphism did not affected the Helvetic domain and the mafic igneous products are mainly concentrated in the Austroalpine-Southalpine domain (Fig. 4, with insets 1, 2, 3, 5 and 10, and Table 3). Gabbros country rocks range from HT-IP metamorphics (granulites: Sills, 1984; Handy and Zingg, 1991; Lardeaux and Spalla, 1991) to consolidated metasediments (Borsi *et al.*, 1968), suggesting that the emplacement took place both in the lower and upper crust. More in detail, rocks recording HT Permian-Triassic metamorphism are in the surroundings of: the Corio and Monastero gabbro (#g1 in Table 3 and inset 1 of Fig. 4) as acidic and basic granulites (#22 in Table 2, and inset 22 of Fig. 1) in the Sesia Lanzo zone; the Dent Blanche gabbros (#g3 in Table 3 and inset 3 of Fig. 4) as acidic and basic granulites (inset 26 of Fig. 1); the Sondalo gabbro (#g5 in Table 3 and inset 5 of Fig. 4) as granulites (#32a in Table 2 and inset 32 in Fig. 1); the Baerofen gabbro (#g6 in Table 3 and Fig. 4) as HT metapelites (#31 in Table 2); the Ivrea gabbros (#g10 in Table 3 and inset 10 of Fig. 4) as granulitized metabasic and metapelites (#36 in Table 2). The calc-alkaline affinity and the orogenic-like signature of the Permian magmatism may result from crustal

TABLE 2
Assemblages and physical conditions of Permian-Triassic metamorphism recorded in the continental crust of the Alps

tectonic system	key	tectonic unit - location	assemblages	lithologies	T(K)	P(GPa)	age (Ma)	method	refs.
PN	19	Briancon basement Ruitor	Ad-bearing metapelites	metapelites	723-823	0.1-0.3	Permian (295-245)	Rb/Sr K/Ar	(1; 2)
PN	20	Monte Rosa	Grt + Sil + Bt + Kfs ± Ms	metapelites			250-280	U/Pb	(3; 4)
PN	21	Dora Maira	Grt + Sil + Bt + Pl + Qtz	metapelites	923-1023	0.4-0.7	pre-Alpine (295-245)		(5)
AU	22a	Sesia Lanzo Zone lower element	Opx + Pl + Grt + Qtz + Hbl	basic granulites	973-1073	0.7-0.9	Permian? (295-245)		(6)
AU	22b	Sesia Lanzo Zone lower element	Sill + Bt + Cd + Pl + Qtz	acidic granulites	973-1023	0.6-0.8	Permian? (295-245)		(6)
AU	23	Sesia Lanzo Zone upper element	Opx + Pl + Grt + Qtz + Hbl Sill + Bt + Pl + Qtz	basic and acidic granulites	973-1023	0.6-0.7	Permian? (295-245)		(7;8;9)
AU	24	Mt. Emilius Klippe	Hbl + Plg + Qtz	metabasics	823-923	0.3-0.45	280?		(10)
AU	25	Mont Mary Nappe	Grt + Sil + Bt + Pl + Ms	metapelites	783-853	0.25-0.45	Permian? (295-245)		(11)
AU	26	Dent Blanche Nappe (Valpelline)	Opx + Pl + Grt + Qtz + Hbl Sill + Bt + Cd + Pl + Qtz	basic and acidic granulites	1023-1073	0.5-0.7	≥ 180	K/Ar	(12; 13; 14)
AU	14b	Silvretta (Pischahorn)	Qtz + Ms + And	metapelites	˜873	˜0.2	>280 (295-280)	K/Ar	(15; 16)
AU	27	Strieden Kreuzeckgruppe	Sil + Bt + Pl + Qtz + L	metapelites	873-1023	0.3-0.5	261 + 3 229 + 3	Sm/Nd	(17; 18)
AU	28	Uttenheim Ahrntal	Grt + Bt + Sil + Pl + Qtz + L	metapelites	893-953	0.5-0.7	262 + 7 253 + 7	Rb/Sr Sm/Nd	(19; 20; 18)
AU	29	Matsch Nappe	Grt + Sil/And + Bt ± Crd + Pl + Qtz	metapelites	843-913	0.3-0.55	290 + 17	Rb/Sr	(21; 22)

AU	30a	Woelz Complex	Grt + Chl + Ms/Pg + Ab + Qtz ± Bt ± Mrg	gneiss	713-793	0.2-0.4	220-260	Rb/Sr	(23)
AU	30b	Woelz Complex	Grt + Bt + Ms +Ilm/Rt + Pl + Qtz	metapelites	788-828	0.35-0.45	Permian (295-245)		(24)
AU	31	Saualpe-Koralpe	Grt + Bt + Sil + Pl + Qtz	metapelites	570-610	0.3-0.4	267 + 17	Sm/Nd	(25)
AU	32a	Languard-Campo	Sil + Opx +Kfs + Bt + Qtz	granulites	843-1023	0.4-0.6	˜290	Sm/Nd	(26; 27; 18)
AU	32b	Languard-Campo	Cd + Bt + Grt + Sp + Sil + Qtz	granulites-contact metamorphism	1123-1223	0.4-0.6	˜290	Sm/Nd	(28; 27)
AU	33	Languard-Campo	Sill + Bt + Grt + Cd + Pl + Qtz Hbl + Grt + Cpx + Pl + Qtz	metapelites and metabasics	923-1093	≤ 0.5	260-280	Rb/Sr	(29; 30)
SA	34	Eisacktal	Crd + Sil + Bt	metapelites-contact metamorphism	≤902	≤0.26	282		(31; 32)
SA	35	Strona-Ceneri Zone	Sil-, Ad-, Crd-bearing metapelites	metapelites			Permian		(33; 18)
SA	36a	Ivrea Zone	Sill + Bt + Grt + Cd + Pl + Qtz	metapelites	953-1053	0.45-0.65	250-290		(34; 35; 36; 37; 38)
SA	36b	Ivrea Zone	Grt + Opx + Hbl +Pl + Qtz	metabasics	1023-1223	0.8-0.9	273-296		(39; 37; 38)
SA	37	Dervio Olgiasca Zone	Bt+Sil+Pl+Qtz±Grt±Kfs AmpII ± Cpx + Pl + Qtz ±Bt	metapelites metabasics	923-1023	0.4-0.6	224-228	Rb/Sr	(40; 41; 42; 43)

Radiometric estimates are expressed as age intervals which represent the minimum and maximum values of the error bar (the dating method is specified in the column Method). The age indication based on geological constrains is expressed in brackets and the column Method is empty. Key as in Fig. 1 and $T_{max}P_{Tmax}$ values are represented in Fig 3; PN: Penninic Domain, AU: Austroalpine Domain, SA: Southalpine Domain. Reference key: 1= Desmons, 1992; 2= Bocquet *et al.*, 1974; 3= Engi *et al.*, 2001; 4= Dal Piaz, 2001; 5= Bouffette *et al.*, 1993; 6= Lardeaux and Spalla, 1991; 7= Lardeaux, 1981; 8= Vuichard, 1987; 9= Biagini *et al.*, 1995; 10= Dal Piaz *et al.*, 1983; 11= Pennacchioni and Cesare, 1997; 12= Nicot, 1977; 13= Hunziker *et al.*, 1992; 14= Gardien *et al.*, 1994; 15= Brugger, 1994; 16= Maggetti and Flish, 1993; 17= Hoke, 1990; 18= Schuster *et al.*, 2001; 19= Stoeckhert, 1987; 20= Borsi *et al.*, 1980; 21= Gregnanin, 1980; 22= Haas, 1985; 23= Schuster and Frank, 2000; 24= Gaidies *et al.*, 2006; 25= Habler and Thoeni, 1998; 26= Giacomini *et al.*, 1999; 27= Tribuzio *et al.*, 1999; 28= Gosso *et al.*, 1995; 29= Spalla *et al.*, 1995; 30= Zucali, 2001; 31= Visonà, 1995; 32= Benciolini *et al.*, 2006; 33= Boriani and Burlini, 1995; 34= Hunziker and Zingg, 1980; 35= Brodie *et al.*, 1989; 36= Quick *et al.*, 1992; 37= Vavra *et al.*, 1996; 38= Colombo and Tunesi, 1999; 39= Henk *et al.*, 1997; 40= Diella *et al.*, 1992; 41= Bertotti *et al.*, 1993; 42= Sanders *et al.*, 1996; 43= di Paola and Spalla, 2000.

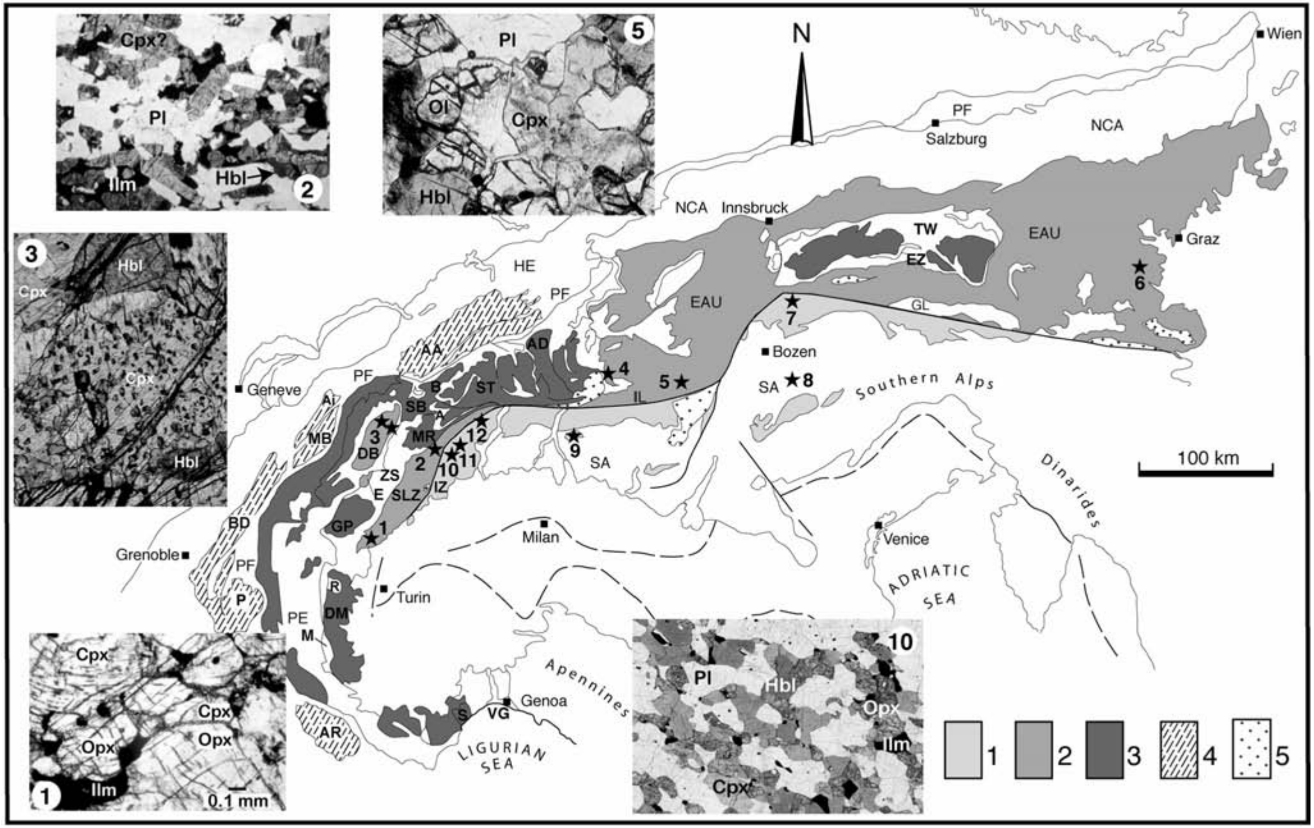

Fig. 4 – Tectonic map of the Alps with distribution of the main Permian-Triassic gabbros (black stars), emplaced in the pre-Alpine continental crust. Labels are as in Table 3. The label of the photomicrographs corresponds to the sample location on the tectonic map. 1: granoblastic texture in the Corio-Monastero gabbros, Sesia-Lanzo Zone, Western Austroalpine (Rebay and Spalla, 2001). Small new grains of Opx, Cpx and Hbl form during HT recrystallization, accompanying pre-Alpine gabbro exhumation. Plane polarized light, long side of the photomicrograph ≈1.4 mm. 2: hornblende-bearing Permian gabbro from Val Sermenza with well preserved igneous texture; photomicrograph in plane polarized light modified after Venturini (1995). 3: Poikilitic Cpx and brown Hbl in the granoblastic texture of the Collon gabbro, Dent Blanche Nappe, Western Austroalpine. Crossed polarisers, long side of the photomicrograph ≈5 mm. 5: idiomorphic Pl in Ol-Cpx-Hbl-bearing Sondalo gabbro, Austroalpine Domain, Central Alps. Plane polarized light, long side of the photomicrograph ≈4 mm; 10: granoblastic texture in a Hbl-bearing gabbro from the Ivrea Zone, Southalpine Domain, Western Alps. Plane polarized light, long side of the photomicrograph ≈ 15 mm. Mineral abbreviations from Kretz (1983). Legend as in Fig. 1.

TABLE 3
Main Permian-Triassic gabbros emplaced in the continental crust of the Alps

tectonic system	key	location	lithologies	Material	Method	Age (Ma)	refs.
AU	1	Sesia Lanzo - Corio and Monastero	gabbro-norite		geological evidences	Permian?	(1)
AU	2	Sesia Lanzo - Sermenza	gabbro	Zrn	U/Pb	288+2/-4	(2)
AU	3	Dent Blanche - Matterhorn Collon	gabbro	Phl	K/Ar Rb/Sr	250±5	(3)
AU	3	Dent Blanche - Matterhorn Collon	gabbro	Zrn	U/Pb	284 ±0.6	(4; 5)
AU	3	Dent Blanche - Mont Collon Dents de Bertol	mafic dykes (alkaline lamprophyres)	Prg	Ar/Ar	˜260	(4; 5)
AU	4	Fedoz-Braccia	gabbro	Zrn	U/Pb	266-276	(6)
AU	4	Fedoz-Braccia	gabbro	Zrn	U/Pb	281±19 281±2	(7; 8)
AU	5	Sondalo	gabbro (?)	Bt	Rb/Sr	242±4	(9)
AU	5	“	troctolite	Pl-Amp-Cpx-WR	Rb/Sr Sm/Nd	266±10; 300±12	(10)
AU	5	“	norite	Pl-Amp-WR	Rb/Sr Sm/Nd	269±16; 280±10	(10)
AU	6	Baerofen	gabbro	Cpx,Pl,WR	Sm/Nd	275±18	(11)
AU	6	“	“		Sm/Nd	261±10	(11)
AU	6	Baerofen and Gressenberg	eclogitised gabbro	Pl-Cpx	Sm/Nd	247±16; 255±9	(12)
SA	7	Bressanone	gabbronorite	Bt	Rb/Sr	276±4	(13; 14)
SA	8	Monzoni	gabbro	Bt	Rb/Sr	225-234	(15; 16)
SA	8	Predazzo	gabbro, diorite	Zrn Bt, Amp	U/Pb Ar/Ar	232-238	(17; 18; 19)
SA	9	Val Biandino	gabbrodiorite	WR	Rb/Sr	279±5	(20)
SA	10	Ivrea - Val Sesia, Val Mastallone	gabbro-diorite	Zrn	U/Pb	285	(21)
SA	10	Ivrea - Valbella Sassiglioni	gabbro	Grt-WR	Sm/Nd	271±22	(22)
SA	10	“	“	Grt-Pl-WR	Sm/Nd	248±8	(22)
SA	10	Ivrea - Val Sessera	gabbro	Cpx,Opx,Pl	Sm/Nd	274±11	(23)
SA	10	“	“	Amp,WR	Sm/Nd	267±21	(23)
SA	11	Ivrea - Val Strona	metabasics	Zrn	U/Pb	293±6	(24)
SA	12	Ivrea - Finero	gabbro	Grt,Cpx,Pl,Amp	Sm/Nd	215±15	(25)

Radiometric estimates are expressed as age intervals, which represent the minimum and maximum values of the error bar (the dating method is specified in the column Method). The age indication based on geological constrains is expressed in brackets and the column Method is empty. Key as in Fig 4; AU: Austroalpine Domain; SA: Sothalpine Domain. Reference key: 1= Rebay and Spalla, 2001; 2= Bussy *et al.*, 1998; 3= Dal Piaz *et al.*, 1977; 4= Monjoie *et al.*, 2004; 5= Monjoie *et al.*, 2005; 6= Muentener *et al.*, 2000; 7= Hansmann *et al.*, 2001; 8= Hermann and Rubatto, 2003; 9= Del Moro in Boriani *et al.*, 1985; 10= Tribuzio *et al.*, 1999; 11= Thoeni and Jagoutz, 1992; 12= Miller and Thoeni, 1997; 13= del Moro and Visonà, 1982; 14= Visonà, 1995; 15= Borsi *et al.*, 1968; 16= Povoden *et al.*, 2002; 17= Mundil *et al.*, 1996; 18= Visonà, 1997; 19= Ferry *et al.*, 2002; 20= Thoeni *et al.*, 1992; 21= Pin, 1986; 22= Voshage *et al.*, 1987; 23= Mayer *et al.*, 2000; 24= Vavra *et al.*, 1999; 25= Lu *et al.*, 1997.

contamination of basaltic magmas derived from enriched lithospheric and/or astenospheric mantle sources. Lithospheric extension and attenuation favoured simultaneous production of lithospheric and/or astenospheric magmas (Cortesogno *et al.*, 1998). Pegmatite emplacement clusters at ≈225 Ma in the Southalpine crust, but it takes place also in the Austroalpine continental crust, in the same time interval (Ferrara and Innocenti, 1974; Staehle *et al.*, 1990; Sanders *et al.*, 1996; Schuster *et al.*, 2001).

On the base of the above described data, the older metamorphic and magmatic radiometric ages of Permian-Triassic time can be interpreted as representing metamorphic and igneous markers of the earlier stages of Mesozoic rifting (e.g Lardeaux and Spalla, 1991; Quick *et al.*, 1992; Dal Piaz, 1993), whereas the younger ages can be interpreted as minimal ages of thermal pulses during extension-related decompression (Vavra *et al.*, 1999), or as due to a late regional thermal event (Lu *et al.*, 1997).

Modelling

To understand the geodynamic settings at the transition between Variscan convergence and Permian-Triassic HT metamorphism we use finite element techniques to model the lithospheric detachment process during continental convergence. Our modelling includes the deep heterogeneities of the mantle, generated by previous oceanic subduction, which consumed a 2500 km wide ocean during a 50 Ma convergence from 425 to 375 Ma (e.g. Tait *et al.*, 1997; von Raumer *et al.*, 2003).

The continuity

$$\nabla \cdot \vec{v} = 0, \qquad (1)$$

momentum

$$\frac{\partial \tau_{ij}}{\partial x_j} = \frac{\partial p}{\partial x_i} - \rho\vec{g}, \qquad (2)$$

and energy

$$\rho c\left(\frac{\partial T}{\partial t} + \vec{v} \cdot \nabla T\right) = -\nabla \cdot (-K\nabla T) \qquad (3)$$

where $\vec{v}$ is the velocity, ρ the density, p the pressure, the gravity acceleration, τ_{ij} the deviatoric stress tensor, c the thermal capacity at constant pressure, T the temperature and K the thermal conductivity; equations are integrated within a rectangular domain of varying size, in which the flow is driven by velocity boundary conditions and by density contrasts. The 2D finite elements code SubMar (Marotta *et al.*, 2006) is used for the analysis.

Three major model types will be discussed here, characterized by the following common features:

- An incompressible viscous fluid is assumed with temperature dominated viscosity

$$\mu(T) = \mu_o e^{\frac{Ea}{R}\left(\frac{1}{T} - \frac{1}{To}\right)}$$

- Density is assumed to vary with temperature and composition such as

$$\rho = \rho_o\left[1 - \alpha\left(T - T_o\right)\right] + \Delta\rho\, C$$

where μ is the viscosity, μ_0 is the reference viscosity at the reference temperature T_o, Ea is the activation energy, T is the temperature, α is the thermal expansion factor and C is a non-dimensional function describing composition changes and is equal to 0 for pure mantle and to 1 for pure crust.

- The crust is compositionally differentiated from the mantle by using the Lagrangian particle technique (e.g., Christensen, 1992). At the beginning of the deformation history, a certain amount of markers (depending on the model type) are distributed to distinguish the crust from the mantle in the different domains. The position of the individual markers, during the dynamic evolution of the system, is calculated by solving the equation $d\vec{x}/dt = \vec{v}$ using a Runge-Kutta scheme, with $\vec{x}$ and $\vec{v}$ indicating the position and the velocity of each particle.

- Complexities, such as phase transition at 410 km or phase changes of subducting crustal material, are not taken into account.

- Two tectonic phases are considered: a) active convergence with subduction of oceanic lithosphere and closure of a 2500 km wide ocean; b) purely gravitational sinking of the subducted slab.

Model Type 1

For this type of model (now on called T_1) the 2-D domain, where the numerical solution is performed, extends from 0 km to 600 km in the horizontal direction and from 0 to 640 km in depth (Fig. 5, panel a). Numerical calculations are performed over an irregular grid composed of quadratic 6-node triangular elements, with a denser nodal distribution near the surface. The initial configuration of the model corresponds to a stratified 80 km thick lithosphere with an initial 10 km thick crust in the oceanic area, from 0 km to 200 km, and 30 km thick crust in the continental area, from 200 km to 600 km, in the horizontal direction. No compositional distinction between continental and oceanic crust is done. Parameters used in the analysis are listed in Table 4. In order to account for an ocean 2500 km wide and for a further approaching continent, we distribute markers outside the numerical grid, with a density of 1 marker/4 km^2: from -2700 km to -2300 km along the horizontal direction and from 80 km depth to surface, to define an incoming continent, and from -2300 km to 0 km and from 80 km depth to surface, to define the remnant oceanic lithosphere. While the base of the crust is defined compositionally, the base of the lithosphere is defined thermally by the isotherm 1600 K which reflects the thickness of a 60 Ma old oceanic lithosphere (Turcotte and Schubert, 2002). Although lithospheric mantle is not compositionally distinguished from sub-lithospheric mantle, in this type of model markers are used to identify also the lithospheric mantle. This allows following the paths of lithospheric mantle particles during the dynamic evolution of the system. Thermal and velocity boundary conditions for the active convergence and purely gravitational sinking phases are summarized in Fig. 5 b-c. During the active convergence phase, until the closure of the ocean and the beginning of continental collision, all the crustal and mantle markers, located outside the 2-D numerical grid, are forced to move with a velocity equal to the convergence velocity prescribed at surface.

Fig. 6 shows the velocity and temperature fields predicted by model T_1 throughout the simulation, lasting 200 Ma from the beginning of convergence, assumed at the absolute age of 425 Ma. During oceanic subduction the mantle flow is controlled by the active tectonic forces responsible for the closure of the ocean. The ablative character of subduction drives the pealing of both crust and mantle material from the overriding continent and its sinking to great depths (Fig. 6a). After 50 Ma of oceanic subduction, when continental collision begins, mantle flow is still controlled by the active tectonic forces (Fig. 6b). At this time the ocean is consumed and most part of the oceanic mantle is involved into the wide scale mantle convective flow.

During the active oceanic subduction phase, the limited horizontal wideness of the study domain and the rather high lithosphere viscosity prevent the development of a local convective cell below the overriding plate, where mass transport is mainly horizontal. As a consequence, during this first stage of evolution a rather thick subduction zone develops, as enlighten by the red and pink markers in Fig. 6a-c.

1 Ma after the cessation of active convergence (Fig. 6c), the system starts to decelerate and flow is mainly controlled by density contrasts. Flow resembles a typical convective pattern, with the largest cell below the lower plate, while a secondary convective cell develops below the upper plate. With the progress of purely gravitational evolution (Fig. 6d), the convective cells become comparable. The lower plate is significantly thinned by the erosion effect driven by the largest convective cell. The collision front migrates towards the upper plate about 100 km. The lithospheric root is thermally softened and thinned. 105 Ma after active convergence ceased (Fig. 6e), collision front reaches its maximum displacement and the upper plate lithosphere begins to thin. The thermal detachment of the lithospheric root is totally accomplished. At the final stage of the simulation, 145 Ma after active convergence ceased (Fig. 6f), the lithospheric root is completely thermally detached and the collision front retreats towards the lower plate, while the upper plate lithosphere continues to thin.

Fig. 7 shows the surface horizontal velocities (Fig. 7a) and the associated surface horizontal strain rate (Fig. 7b-f) during the oceanic subduction, between 425 and 375 Ma, and after continental collision, until 230 Ma, when dynamics is controlled by solely gravitational forces. Due to the boundary conditions assumed during the active oceanic subduction (Fig. 5b), lithosphere behaves, at

Table 4
Material properties used in T_1 and T_2 numerical modelling

	Crust	Mantle
Mean density (kg/m^3)	3000	3200
Thermal conductivity (W/mK)	3.4	
Heat generation (10^{-6} W/m^3)	0	
Rheology	Newtonian fluid	
μ_o Pa s^{-1}	0.5×10^{21}	
A (K^{-1})	4.60517	

surface, like a rigid plate and no surface horizontal strain rate is definable. During the initial stage of the purely gravitational phase the dominant positive buoyancy forces, associated with the cold subducted slab, and the free slip conditions, assumed at the upper boundary of the system, induce a strong horizontal extension throughout the surface of the upper plate (Fig. 7b and 7c). The deformation style at the surface of the old upper plate varies from dominant widespread horizontal shortening to alternating horizontal shortening and extension, with extension starting between 70 and 80 Ma after the onset of continental collision (at ~300-290 Ma absolute time; see also Fig. 7d and 7e) and concentrating near the suture zone. Magnitude of horizontal extension increases in time and may lead to breaking of the continental lithosphere and consequent oceanisation in the old upper plate. It is worth to note that horizontal extension in the old upper plate starts immediately

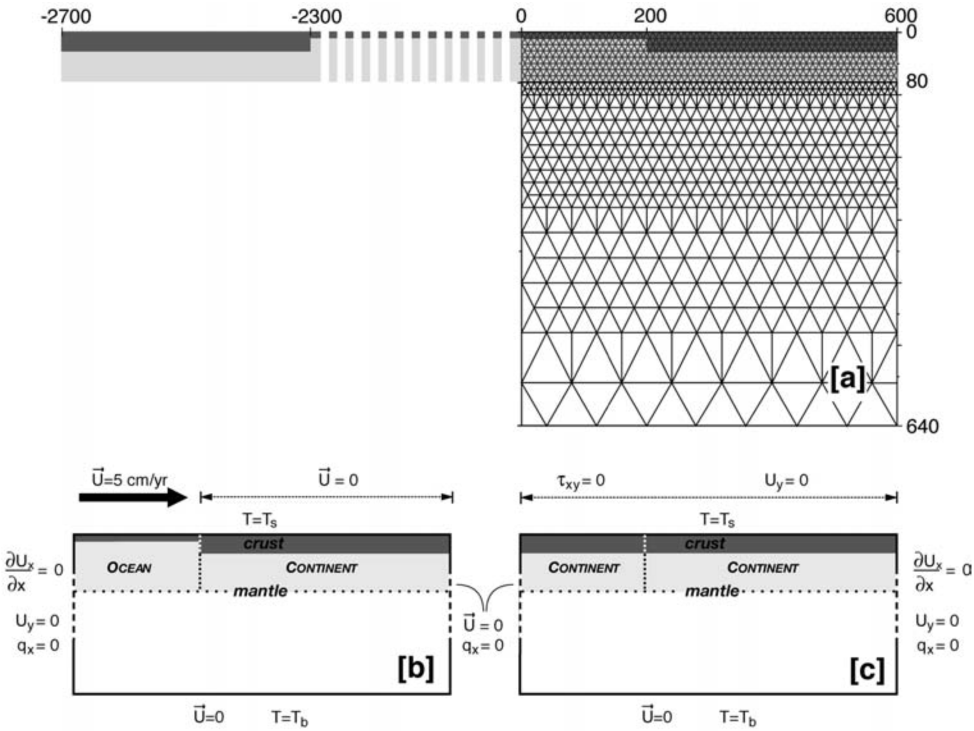

Fig. 5 – (a) 2D geometry and numerical setup of model T_1. Distance, in km, is not in scale. (b) and (c) Thermal and velocity boundary conditions used for model T_1 during the active oceanic subduction (b) and the collisional and post-collisional phases (c), respectively.

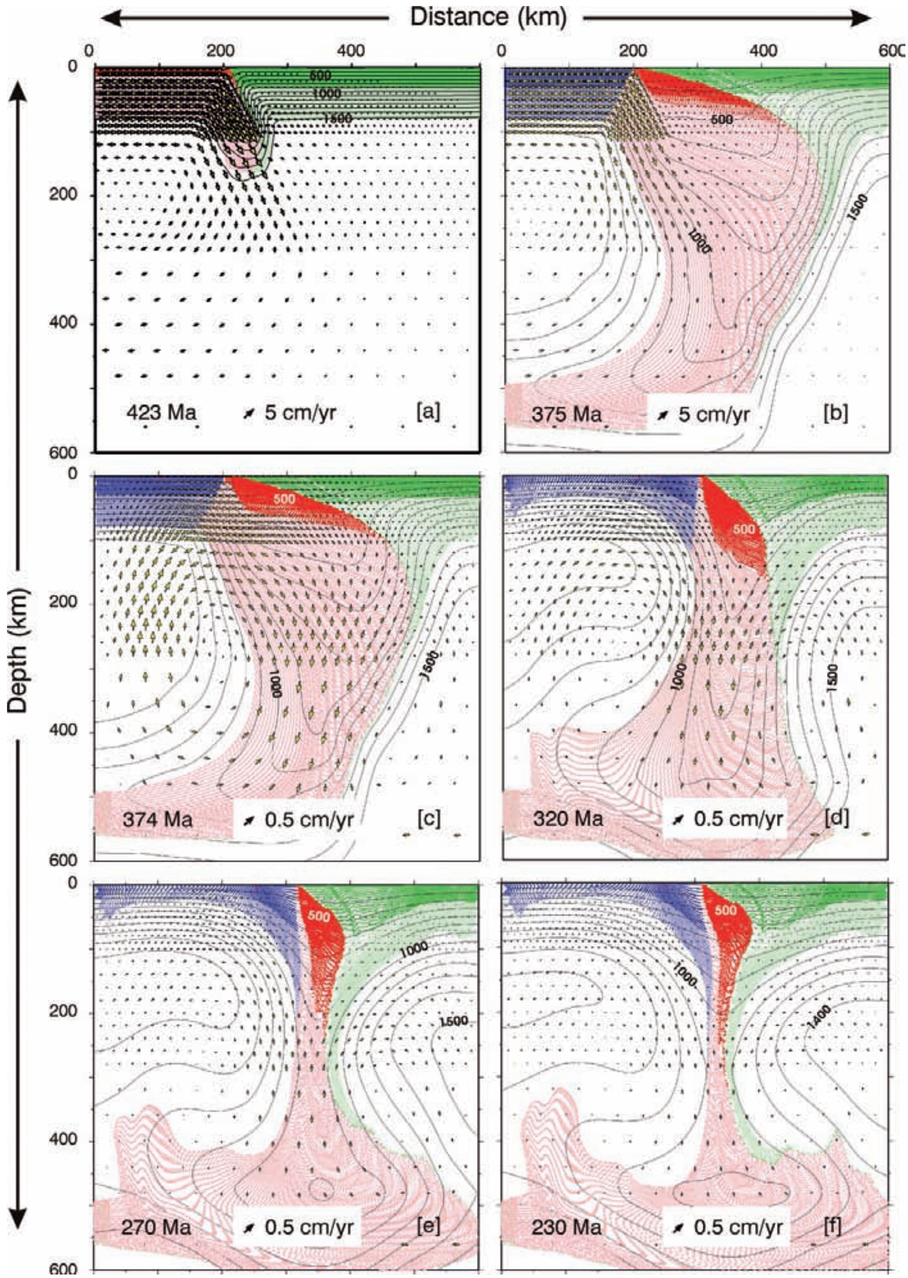

Fig. 6 – Thermal (continuum lines) and velocity (yellow arrows) fields predicted by model T_1 after 2 Ma (a) and 50 Ma (b) from the beginning of active oceanic subduction and after 1 Ma (c), 55 Ma (d), 105 Ma (e) and 145 Ma (f) after the cessation of active convergence. Ages indicated on each panel are absolute. Points indicate markers identifying crust (lower plate: blue colour for the continental portion and red colour for the oceanic portion; continental upper plate: green colour) and mantle (lower plate: light blue colour for the continental portion and pink colour for the oceanic portion; continental upper plate: light green colour).

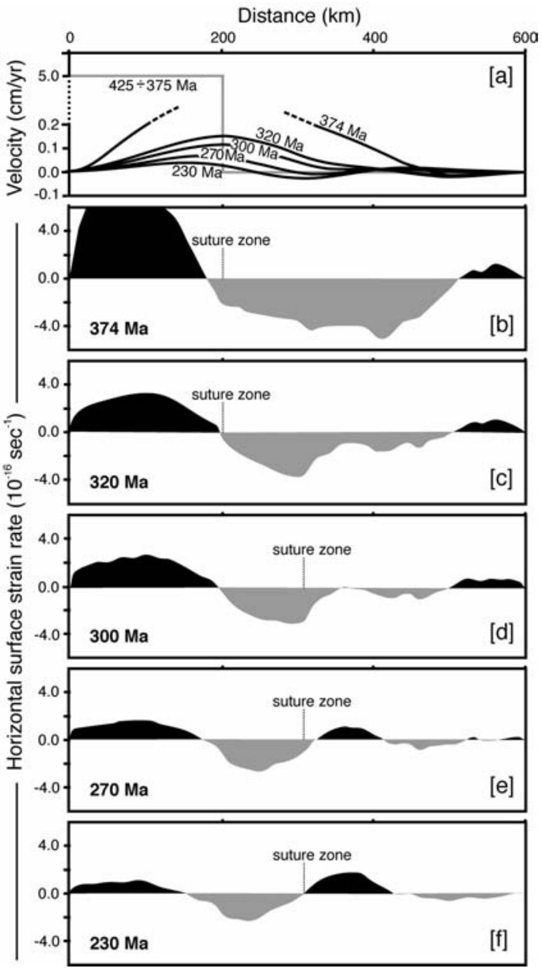

Fig. 7 – Variation of surface horizontal velocities predicted by model T_1 during the active oceanic subduction phase (grey solid line) and the post-collision phase (black solid lines) (panel a); variation of the corresponding horizontal surface strain rate (b - f). Black stands for extension (positive values) and grey stands for shortening (negative values). The varying position of the suture zone during the evolution of the system is shown. Ages indicated on each panel are absolute.

after the thermal detachment, and its magnitude increases in time. Reversely, in the lower plate the magnitude of the horizontal surface strain rate decreases in time.

From results of model T_1 some consequences can be deduced:

a. Thermal detachment of the lithospheric root occurs 105 Ma after the onset of continental collision (at ~270 Ma absolute time).

b. Upper plate horizontal extension starts between 0 and 80 Ma after continental collision. It increases in time.

c. Variation of surface horizontal strain rate locates the region where horizontal extension may develop above the major thermal lithosphere thinning, induced by mantle up-welling, below the old upper plate.

d. The individuation of an extensional domain of increasing magnitude located on the old upper plate, close to the Variscan suture zone, and the correspondent tendency of the system to warm up under there suggest that if the rifting is promoted by the late orogenic Variscan dynamics, it must occur in the Variscan upper plate.

Although promising, this model is affected by several limitations. It does not allow the development of a well-defined mantle wedge at the suture zone, where mantle and crustal material can be recycled and, eventually, exhumed after it has been deeply buried. Furthermore model T_1 is globally too cold and a reasonable comparison between predicted and natural P-T data is not possible. We think that this last aspect, in particular, can be partially related to the limited horizontal extension of the model that does not allow the development of a convective current below the old upper plate, where conduction dominates over convection in the heat transfer process. Consequently, a significant thermal and material thickening of crust and lithosphere mantle occurs, especially during the initial phase of active subduction. Another limitation of model T_1 is the non-differentiation between oceanic crust and continental crust that differ only for their initial thickness (10 km for oceanic crust and 30 km for continental crust). Crustal differentiation could induce variations in the buoyancy forces at the local scale of the wedge area, particularly at the beginning of the active ocean subduction, creating the favourable condition for the expected recycling of crustal material.

Model Type 2

In order to overcome the limitations of model T_1 a second kind of model, model T_2, has been developed, differing from model T_1 in the following aspects:

• *An extended geometry*: the 2-D domain, where the numerical solution is performed, now extends from -700 km to 700 km in the horizontal direction and from 0 to 700 km depth, including a 700 km wide continent and a 700 km wide portion of ocean. An irregular grid composed of quadratic 6-node triangular elements, with a denser nodal distribution near the suture zone is adopted. The remnant portion of ocean and the concurrent continent, 700 km wide, are accounted by using markers outside the numerical grid (Fig. 8). A total amount of 12864 markers are now used to identify crust and mantle material.

• *Different thermal constraints*: different temperature values, ranging from 1600 K (as for model T_1) to 2300 K and 2800 K, are assumed at the bottom of the model to favour the convective heat transfer component inside the 2D domain, with a density of 1 marker/4 km^2.

• *Different velocity boundary conditions along the vertical sidewalls*: during the active subduction phase, the right side is maintained impermeable, while, along the left sidewall a portion extending 100 km from surface is kept "open" ($du/dx=0$, $v=0$ conditions), making the inward/outward material flow possible, thus guaranteeing the satisfaction of the continuity condition. During the pure gravitational phase a portion extending 100 km from surface is kept "open" along both vertical sides of the study domain, while the rest of the vertical sidewalls are kept impermeable.

• *Prolongation of active convergence* phase from 51 Ma to 60 Ma up to doubling of continental crust.

Fig. 9 shows the thermal and velocity fields throughout the evolution as predicted by model T_2, from 425 Ma to 365 Ma for the active oceanic subduction, and to 275 Ma for the purely gravitational phase, in absolute age. During the oceanic subduction and closure of the ocean (Fig.9a-g) the mantle flow is remarkably more intense below the upper plate, contributing with the buoyancy forces, to drive the verticalization of the subducted slab. No evident corner flow develops and, although less evident then for model T_1, thermal thickening occurs below the overriding plate, while thermal field in the oceanic area remains unperturbed. After the beginning of continental collision (50 Ma after the beginning of numerical simulation), small-scale convective cells develop throughout the system and the thermal detachment of the subducted slab accomplishes within 20-30 Ma after cessation of active oceanic subduction (Fig. 9h-i). The final stage of evolution, lasting 70 Ma, is characterized by a significant thinning by thermal erosion effect of the lithosphere, with two major focuses of high thermal regime localized along the old upper plate, where hot mantle material rises up.

This behaviour is also evident in Fig. 10, where the distribution of crust and mantle markers is plotted at the same time as for Fig. 9. At the final stage of evolution a huge amount of oceanic material has risen below the old upper plate, where the high thermal regime develops. The particular impermeable boundary conditions adopted on the deep portion of the right sidewall, probably reinforce the upwelling of material compared to model type 1, even if the type 2 domain is larger.

The distribution of horizontal strain rate predicted by model T_2 (Fig. 11) shows a rather different pattern with respect to the one predicted by model T_1. First of all, T_2 induces magnitudes that are half than those of model T_1. The most striking difference is in the style of horizontal deformation. Both models predict an alternation of horizontal shortening and extension above both continental plates, but their locations are different for the different models (compare Fig. 11 with Fig. 7). In particular horizontal extension characterizes the surroundings of the suture zone along both continents. A striking feature of the surface deformation pattern predicted by model T_2 and different from that predicted by model T_1 is the symmetric distribution of horizontal extension and shortening domains with respect to the suture zone. The different prediction of model T_1 can be an artefact generated by the limited width of the system. In addition the magnitude of horizontal extension smoothes in time, in contrast with the predictions of T_1. Note that localisation of surface horizontal extension corresponds to the site in which the deeply subducted material rises up and thermal thinning is maximal (compare Fig. 11 f with Fig. 10 q and r).

The variation in time of the vertical thermal profiles at different distance from the suture zone during the oceanic subduction phase are shown in

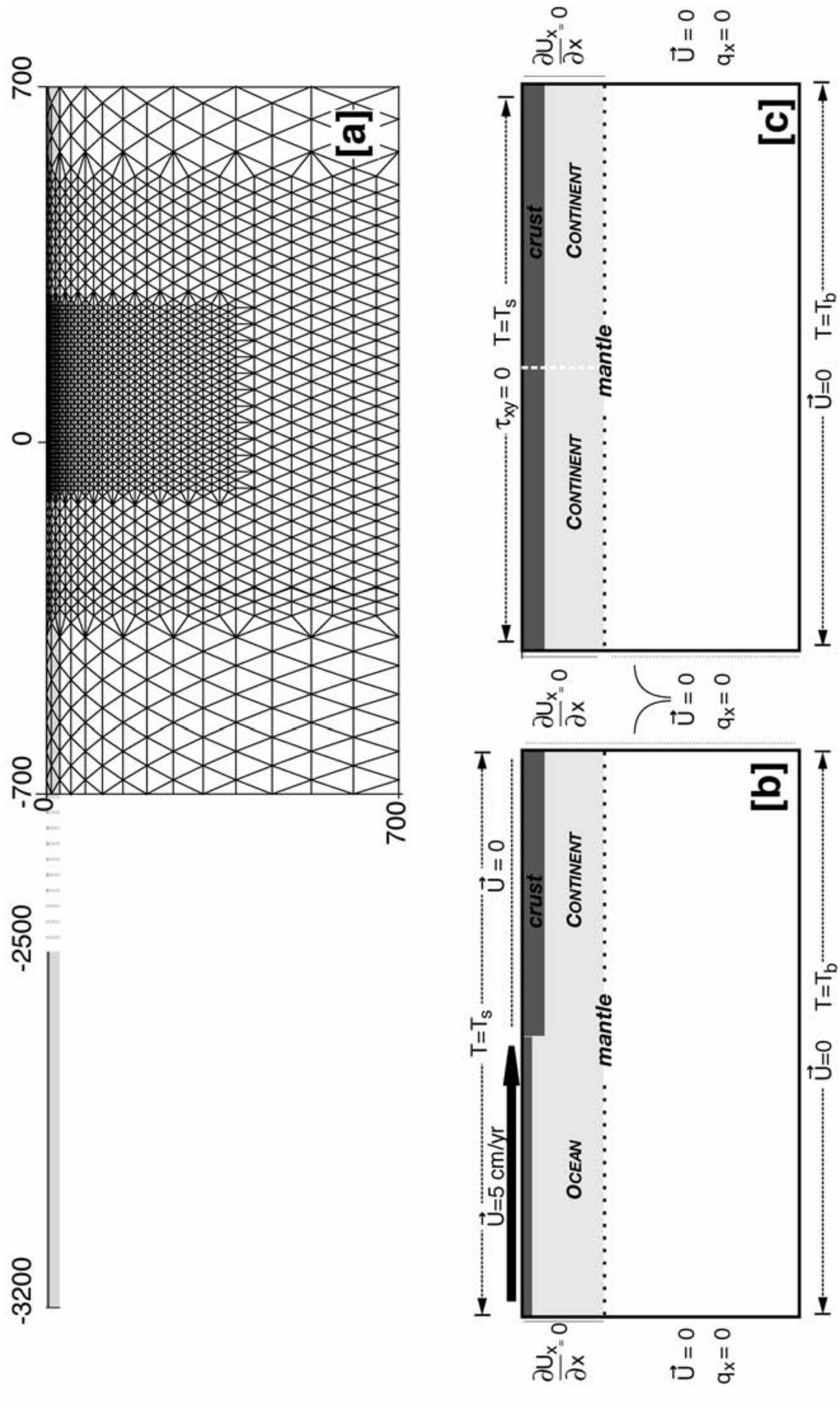

Fig. 8 – (a) 2D geometry and numerical setup of model T_2, (b) and (c) Thermal and velocity boundary conditions used for model T_2 during active oceanic subduction phase (a) and the collisional and post-collisional phases (b), respectively.

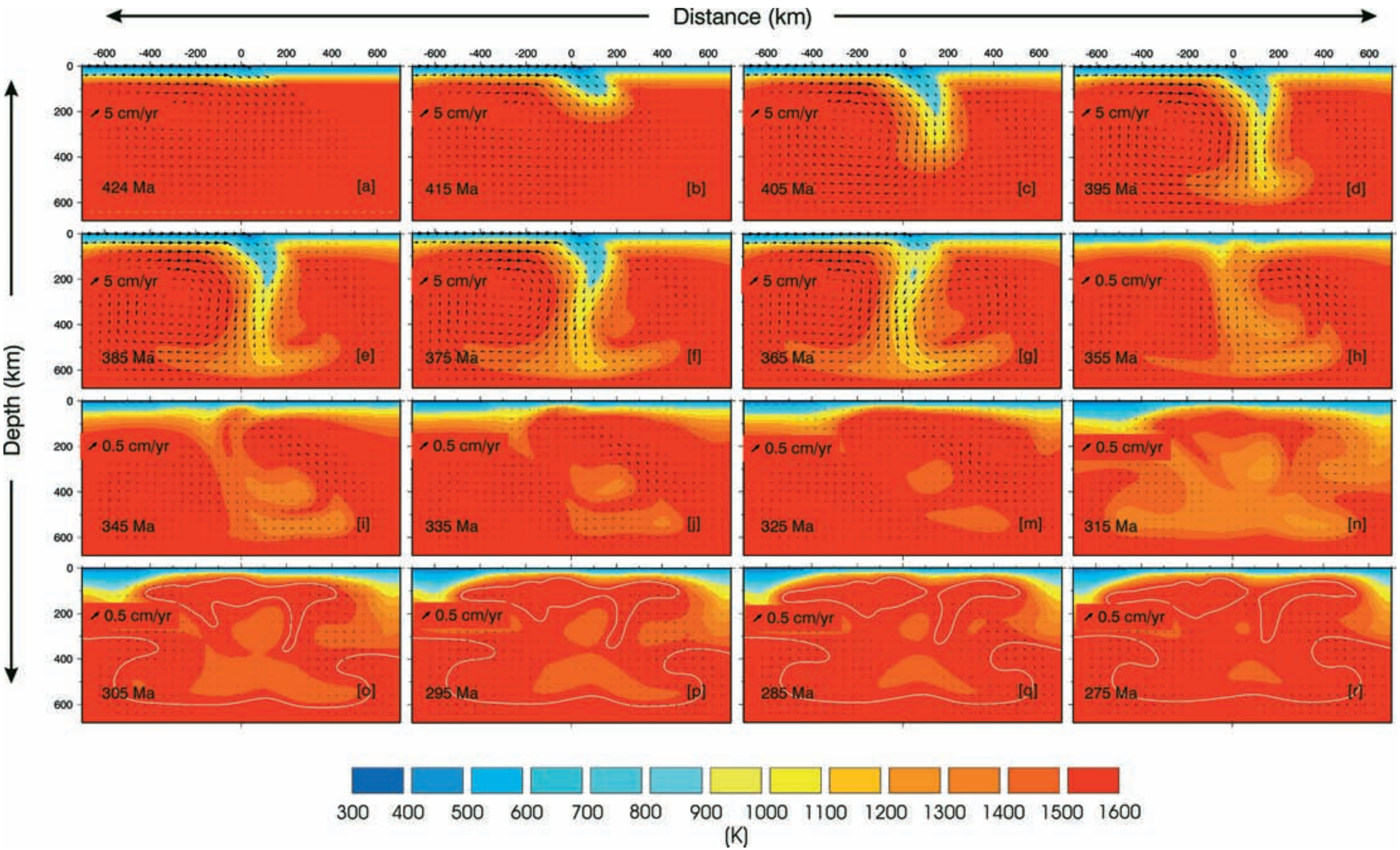

Fig. 9 – Thermal (colour map) and velocity (black arrows) fields predicted by model T_2, after 1 Ma (a), 10 Ma (b), 20 Ma (c), 30 Ma (d), 40 Ma (e), 50 Ma (f) and 60 Ma (g) of active oceanic subduction and after 10 Ma (h), 20 Ma (i), 30 Ma (l), 40 Ma (m), 50 Ma (n), 60 Ma (o), 70 Ma (p), 80Ma (q) and 90 Ma (r) of purely gravitational evolution, after continental collision. Ages indicated on each panel are absolute.

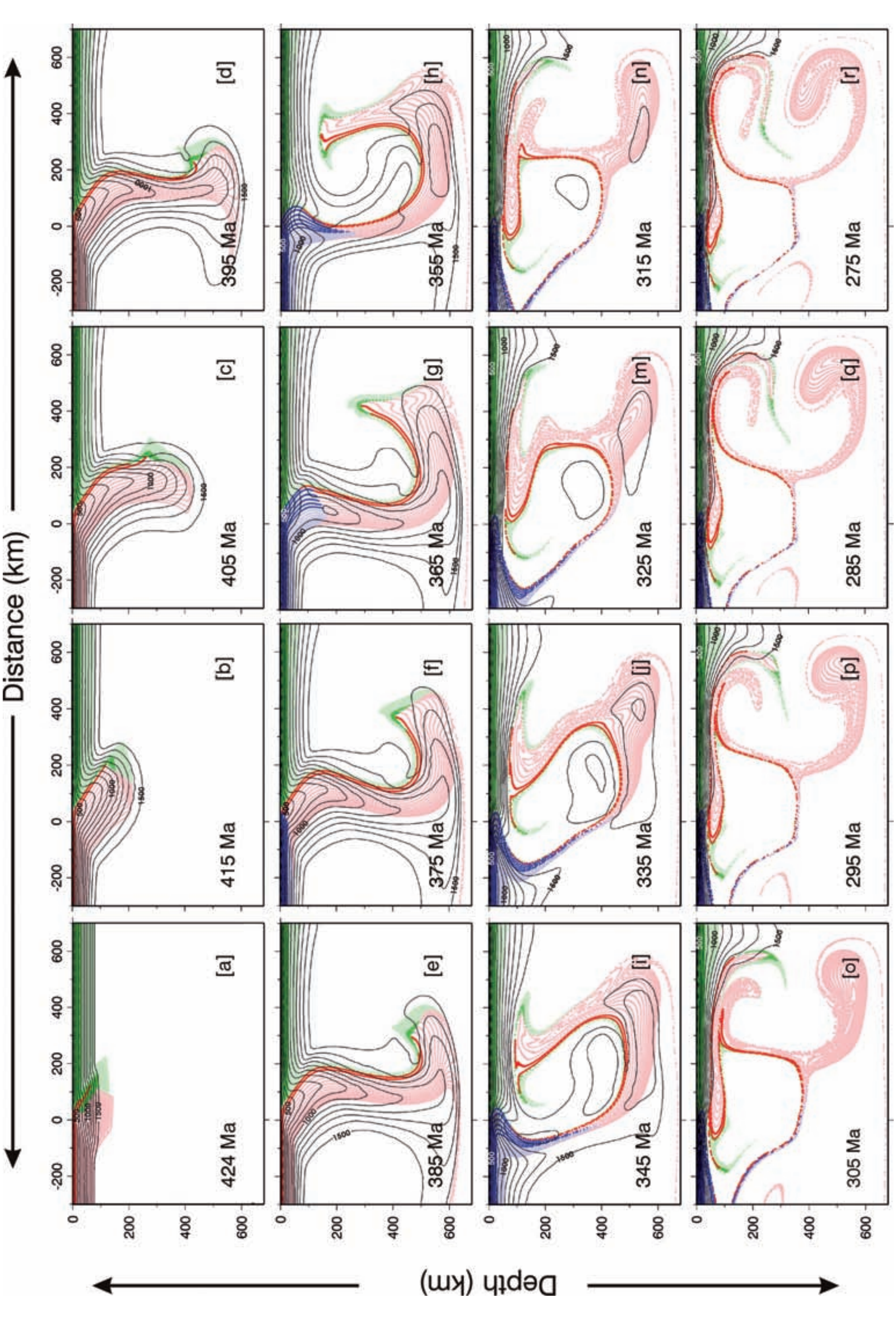

Fig. 10 – Distribution of crust (lower plate: blue colour for the continental portion and red colour for the oceanic portion; continental upper plate: green colour) and mantle (lower plate: light blue colour for the continental portion and pink colour for the oceanic portion; continental upper plate: light green colour) markers predicted by model T_2, at the same time as for Fig. 9 – Ages indicated on each panel are absolute.

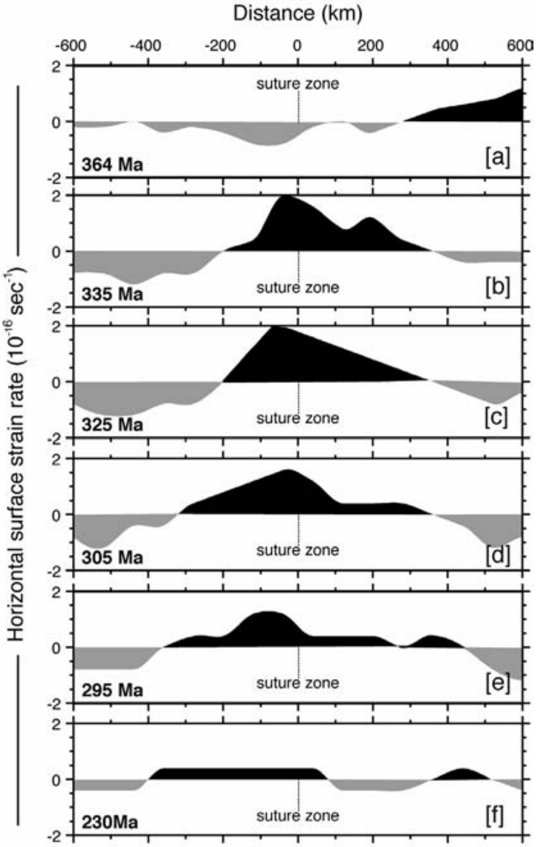

Fig. 11 – Variation of surface horizontal surface strain rate predicted by model T_2 during the post collisional phase. Black stands for extension (positive values) and grey stands for shortening (negative values). The varying position of the suture zone during the evolution of the system is shown. Ages indicated on each panel are absolute.

Fig. 12, which compares them with oceanic and continental crust eclogites and HP rocks of the subduction phase (Table 1). Within the first 10 Ma of oceanic subduction, in proximity of the suture zone through the upper plate, the system undergoes the most striking horizontal and vertical variations in the thermal field (Fig 12a, b and c, at 120, 160 and 200 km far from the suture, respectively). These thermal variations are due to the subduction process that cools the system at depths lesser and lesser while moving from the suture zone. On the contrary, the far field (respect to the suture zone) remains almost unperturbed with respect to the pre-subduction thermal field (black dashed line, Fig. 12d - f). With the progress of active subduction, thermal regime remains rather stable and only a very slow general cooling occurs, within the first 100 km of depth. This characteristic thermal field allows a good thermal fit for data #8 and #11 (Table 1) and within 160 km from the suture zone; thermal conditions suitable for fitting datum #14 (Table 1) are never reached.

A similar comparison between the vertical thermal profiles and the HT-extension related rocks (listed in Table 2) of Permian (grey rectangles) and Triassic age (empty rectangles) at different distances from the suture zone is visible in Fig. 13, along both the old upper and lower plates. During this purely gravitational phase the strongest variations in the thermal field occur in proximity of the suture zone. The general and rapid heating of the system (Fig. 9) is responsible for a lithospheric thinning up to 35 km close to the suture zone (Fig. 13a-b) where lithosphere detachment localized, and up to 65 km between + 120 and + 400 km from the suture zone (Fig. 13c-d). Here lithospheric thinning is engaged by thermal erosion due to large-scale convection (Fig. 9n-r). The final stage of gravitational evolution is characterised by thermal relaxation, more evident far away from the suture zone.

In conclusion, results from model T_2 show that:

a. The high thermal regime results from hot mantle upwelling under the continental plates, leading to thermal thinning and horizontal surface extension, in agreement with the interpretation envisaging an extensional tectonic regime associated with Permian-Triassic thermal high (e.g. Lardeaux and Spalla, 1991; Diella *et al.*, 1992).

b. The uprising of oceanic and continental subducted lithosphere below the old overriding continent strengths model T_1 conclusion that, if the rifting is promoted by the late orogenic Variscan extension, it localises in the Variscan upper plate.

c. Model T_2 shows that the thermal high is induced by the lithospheric unrooting occurring before 335 Ma (less than 40 Ma after continental collision) and persists up to Permian-Triassic times (290 - 225 Ma), high enough to support the fit between natural data and predictions.

In summary model T_2 shows a more effective convective heat transfer and results globally hotter then model T_1, allowing a good thermal fit

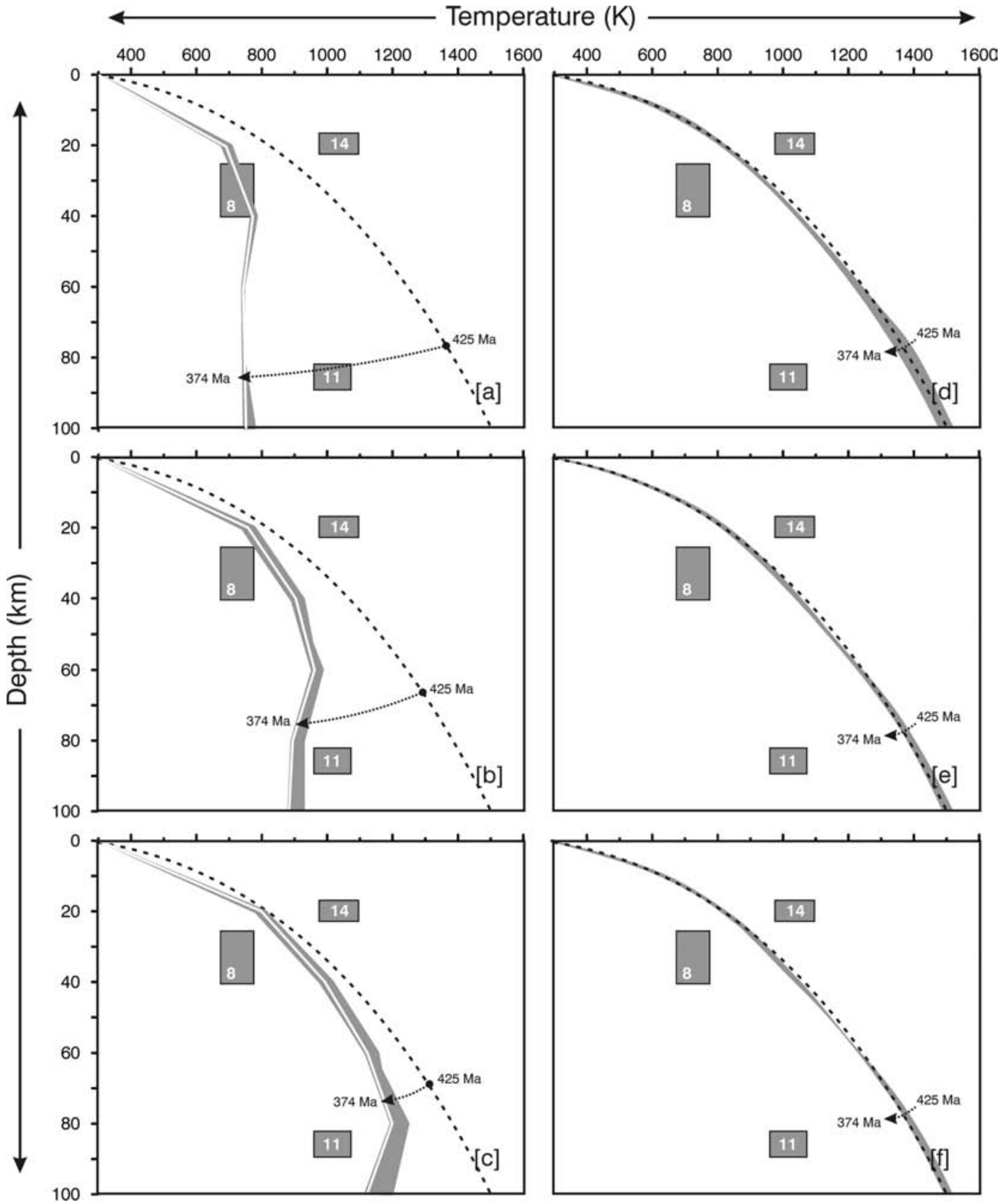

Fig. 12 – Variation in time of the vertical thermal profiles (grey colour) at different distance from the suture zone [+120 km (a), +160 km (b), +200 km (c), +320 km (d), +360 km, (e), +400 km (f)] during the active oceanic subduction phase, compared with the oceanic and continental crust eclogites and HP rocks of the subduction phase and listed in Table 1. Black dashed lines indicates the geotherm at the beginning of the evolution. Labels near the geotherms indicate absolute ages.

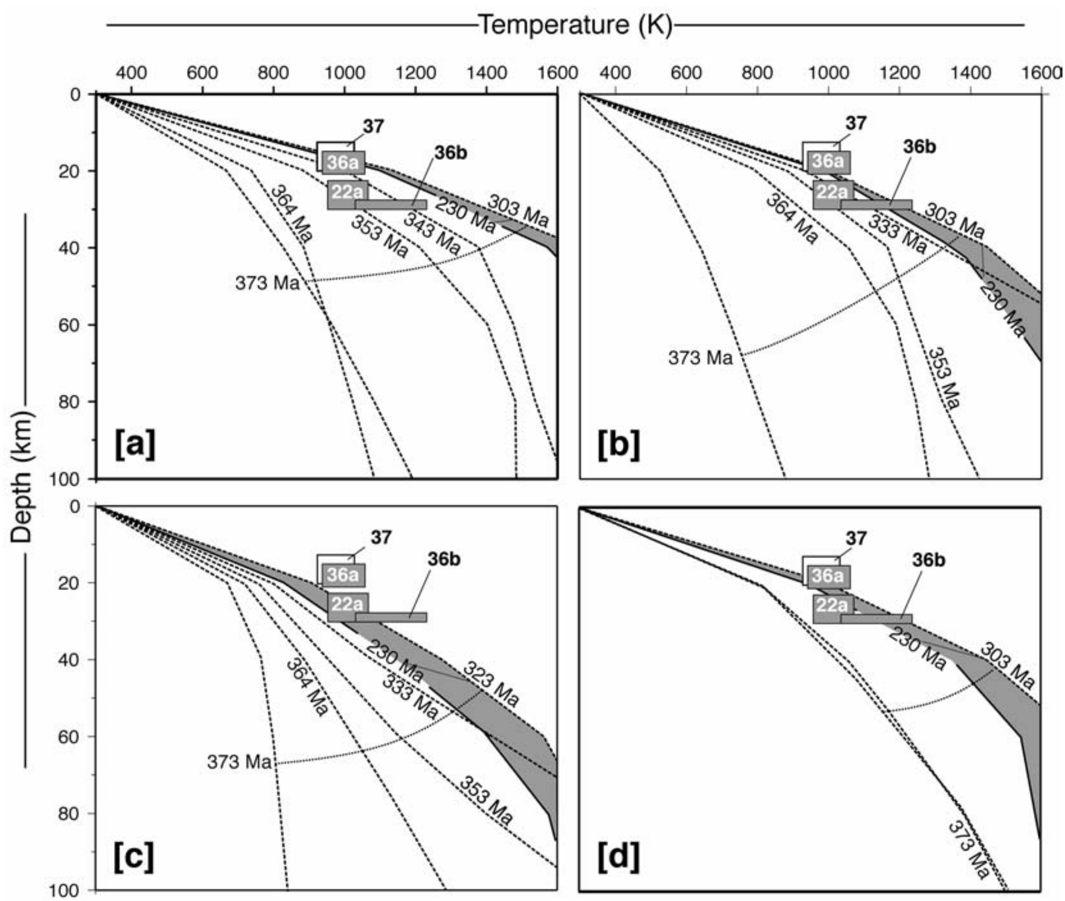

Fig. 13 – Variation in time of the vertical thermal profiles (dashed black lines) at different distance from the suture zone at -40 km (a), +40 km (b), +120 km (c) and +400 km (d) for the post collision phase, compared with HP rocks (listed in Table 2) of the Permian extension age (grey rectangles) and of Triassic extension age (empty rectangles). Grey area corresponds to the envelope of vertical thermal profiles at the comparable age of the HP rocks of the Permian-Triassic extension age. Labels near the geotherms indicate absolute ages.

between prediction and natural P-T data, both for the active convergence phase and for the Permian and Triassic extension phase. However, several forcings still persist in the setup of model T_2, such as the very high temperature fixed at the base of the domain (T_b = 2300 ÷ 2800 K), the zero radioactive heat generation for the mantle and crust, and the lack of a compositional differentiation between continental and oceanic crust.

Model Type 3

Model T_3 is a refinement of T_2 in the following aspects:

- Continental crust is compositionally differentiated from oceanic crust (parameters are listed in Table 5).
- Radioactive heat production is considered both for crust and mantle.

TABLE 5
Material properties used in T_3 numerical modelling

	Continental crust	Oceanic crust	Mantle
Rock components	66% gneiss + 33% granite	7% basalt + 16% dolerite + 77% gabbro	100% dry dunite
Mean density [a] (kg/m^3)	2640	2961	3200
Thermal conductivity [b] (W/mK)	3.03	2.1	4.15
Heat generation [b] (10^{-6} W/m^3)	2.5	0.4	0.002
Rheology	dry Granite [c]	dry Diabase [d]	dry Dunite [e]
Activation energy (kJ/mol)	123	260	444
A (Pa^{-n} s^{-1})	7.92X10^{-29}	8.04X10^{-25}	6.31X10^{-17}
n	3.2	3.4	3.41

a) Dubois and Diament (1997), Best and Christiansen (2001) ; b) Rybach (1988); c) Ranalli and Murphy (1987); d) Kirby (1983); e) Chopra and Peterson (1981).

• Both crust viscosity and density depend on both temperature and composition.

• Markers are used only to identify crust.

• Markers density is 1 marker/1 km^2.

Fig. 14 shows the thermal and velocity fields predicted by model T_3 at different times of the active ocean subduction phase (Fig. 14a-b) and of the post collisional phase (Fig. 14c-d). During the initial phase of active convergence a 45° dip subduction is prescribed. By the time, the convective flow progressively intensifies, driving the descent of the subducting oceanic plate and the thermal thinning of the lithosphere that increases by time, in particular at the wedge area. Note that, with respect to model T_2, a clear upwelling of hot mantle material occurs, which induces a significant thermal erosion in the mantle wedge area (Fig. 14a-b). During the phase of pure gravitational evolution, thermal detachment of the cold subducted lithosphere completes within 7 Ma after the initiation of pure gravitational evolution (Fig. 14c). Focusing on the wedge area, the corner flow developed during the active convergence phase suddenly disappears. By the time a large scale convective flow intensifies and expands below the old upper plate, driving a reduction of the shallow dip of the subducted slab and a consequent rising of the associated crustal material to lower pressures and higher temperatures, although the flow within the lithosphere is too slow to change significantly the geometry of the continent-continent interface at the suture zone. Here a highly thinned continental crust persists until the latest stages of the gravitational evolution. At the mature stage of

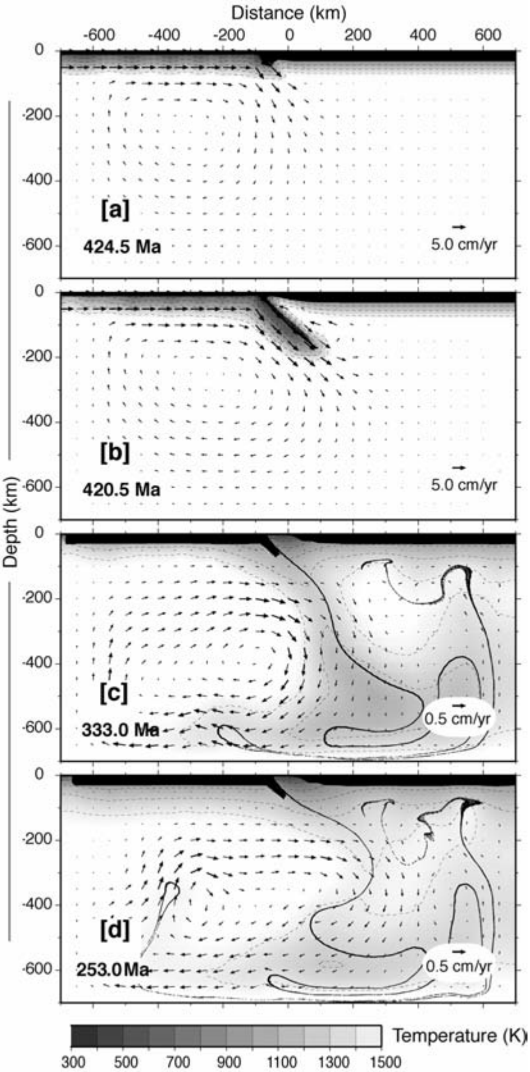

Fig. 14 – Thermal (grey scale and black thin contours) and velocity (black arrows) fields predicted by model T_3, after 0.5 Ma (a) and 4.5 Ma (b) of active oceanic subduction and after 40 Ma (c) and 120 Ma (d) of purely gravitational evolution, after continental collision. Black dots represent crustal type (both continental and oceanic) markers. Ages indicated on each panel are absolute.

the evolution, thermal relaxation of the lithosphere occurs, with consequent approaching of its thermal thickness to the initial value (Fig. 14d).

Looking at the markers distribution in the wedge area (Fig. 15) we note that an *ablative subduction* (e.g. Tao and O'Connel, 1992) occurs and crustal material is scratched from the base of the overriding plate to depth. Crustal erosion affects an area 100 km wide from the trench. The hugest amount of crustal material is eroded within the first 3.5 Ma (Fig. 15a-b), when the local convective flow within the mantle wedge is the most intense. With the subsequent progressive enlargement of the convective flow to the bottom of the study domain, the intensity of the flow inside the mantle wedge diminishes as much as the erosion rate. The erosion ceases at about 25 Ma, when the crustal thinning is maximal (Fig. 15c). Later on, the overriding plate remains almost mechanically stable until continental collision (Fig. 15d). It must be noted that in spite of the intense local mantle flow in the wedge area (Fig. 15b) no crustal material is involved in this small-scale convection and, consequently, recycled at shallow depths.

The velocity field during the pure gravitational subduction phase induces a peculiar strain pattern at surface for the meso-Variscan to Permian period (Fig. 16). Model T_3 predicts alternating domains of horizontal extension and shortening, whose magnitudes decrease in time and with an opposite style with respect to that predicted by model T_2. In particular, the region between - 250 km and + 250 km, comprising the suture zone, is characterized by horizontal shortening, acting both on the upper and lower plates. A second horizontal shortening domain develops along the overriding plate, between 350 km and 500 km. Two major horizontal extensional domains develop from the beginning in proximity of the two vertical borders of the domain and a third one appears at the centre of the overriding plate. At later stages, one single horizontal shortening domain dominates at the middle of the system, although with a very low magnitude with respect to that of the earliest stage. As for model T_2, localisation of surface horizontal extension areas corresponds to the two uprising plumes of deeply subducted material, accompanied by maximum thermal thinning (compare Fig. 11 with Fig. 10).

Fig. 17 shows the variation in time of the vertical thermal profiles (Fig. 17a-f) at different distances from -100 to 100 km around the suture zone (coloured lines and colour bar) during the

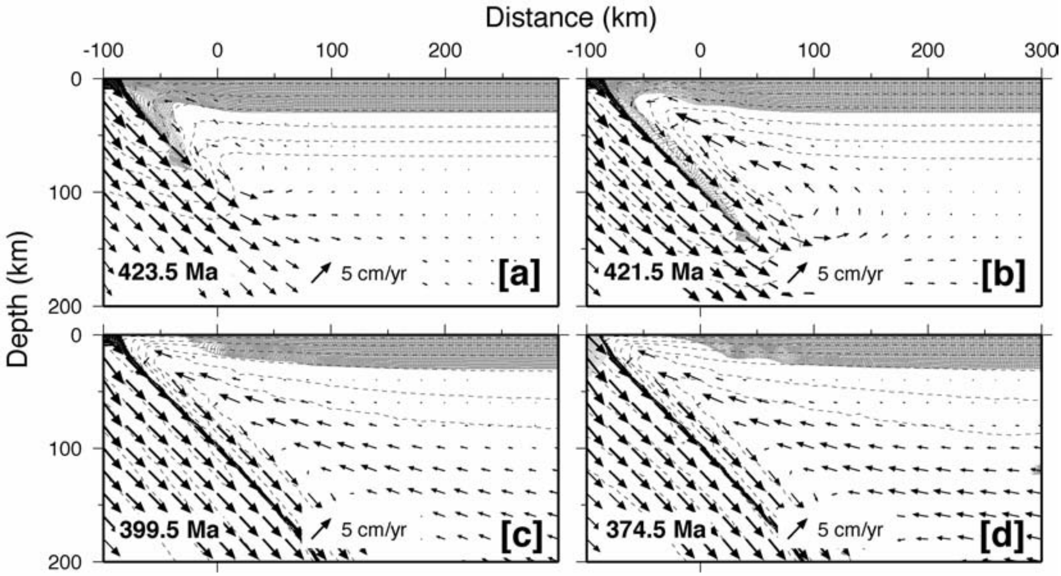

Fig. 15 – Thermal (dotted lines) and velocity fields (black arrows) predicted by model T_3, after 1.5 Ma (a), 3.5 Ma (b), 25.5 Ma (c) and 50.5 Ma (d) of active oceanic subduction. Grey and black points indicate continental and oceanic crust markers, respectively. Ages indicated on each panel are absolute.

active oceanic subduction phase, compared with the natural P-T data from oceanic and continental crust eclogites and related HP rocks (empty rectangles labelled as in Table 1 and Fig. 2). Here P-T conditions of crustal markers from the whole system are plotted in black (oceanic) and ochre (light for the upper continent and dark for the lower continent) and allow to check whether predicted P-T conditions fit P-T estimates on natural rocks in terms of coincidence of age, thermal gradient and compositional affinity (oceanic or continental crust) or simply age coincidence and thermal gradient in the suture zone. Some natural P-T data are satisfied by model predictions only thermally throughout the active convergence phase. This can be a consequence of model assumption that no mantle hydration can occur in the wedge area. Indeed, hydration would enhance local circulation of crustal material, tectonically eroded from the overriding plate, or belonging to the subducting plate, at shallower depths (Gerya and Stoeckhert, 2006 and references therein).

A similar analysis for the collisional to post-collisional phases is illustrated in Fig. 18, where HT metamorphic imprints recorded during Permian and Triassic are plotted as empty rectangles (labelled as in Table 2 and Fig. 4). During the early stages (≥ 330 Ma) of the purely gravitational evolution, the degree of full correspondence between natural data and model predictions is greater than that of the active subduction phase. Successively a progressive decrease of the agreement occurs until it totally disappears during Permian-Triassic times (Fig. 18e-f).

As for models T_1 and T_2, some partial conclusions can be drawn:

a. The agreement between natural data and model predictions, taking into account compositional affinity, age and thermo-baric correspondence, is very good during active convergence and the early stages of purely gravitational evolution, though some complexities, such as phase transitions, have not been taken into account (Marotta and Spalla, 2007).

b. A high thermal regime develops after lithospheric thermal unrooting occurring before 365 Ma, ≈7 Ma after the beginning of continental collision.

c. A positive thermal anomaly persists up to the Triassic but, due to its progressive decrease

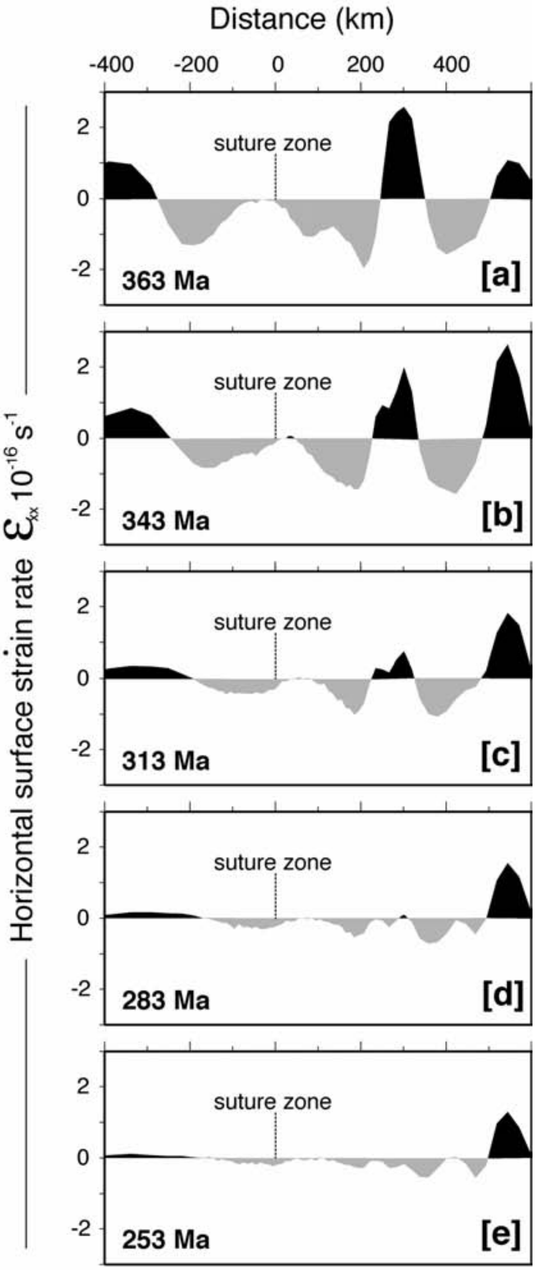

Fig. 16 – Surface horizontal deformation regime from Meso-Variscan to Permian predicted by model T_3. Black stands for extension (positive values) and grey for shortening (negative values). The varying position of the suture zone is shown. Ages indicated on each panel are absolute.

since Permian times, it is never sufficiently high to accomplish the PT conditions inferred from natural data.

d. Surface horizontal strain patterns show that suture zone is characterised by horizontal shortening during the whole purely gravitational evolution, subsequent to collision, with a magnitude decreasing in time. Horizontal extension has been localised in the centre of the old overriding plate since the beginning of the gravitational evolution and is already vanished at the beginning of Triassic. This configuration is opposite with that of model T_2

Conclusions

The comparison among the results of three successive models allow to highlight some main factors controlling the dynamics and thermal evolution of the crustal-mantle system in the Alpine area at the Variscan to Permian-Triassic transition.

All the implemented models indicate that a thermal high is triggered by thermal lithospheric unrooting, which is subsequent to the onset of continental collision. However, the predicted thermal anomaly is high enough to satisfy the PT conditions recorded in the pre-Alpine continental crust during Permian-Triassic period only for model T_2, which accounts for an artfully high temperature at the bottom of the system (2300 K), necessary to sustain the adiabatic gradient in the core of a system in which no radioactive heat production is assumed.

The time span needed to accomplish thermal unrooting is different for the three models, depending on the system horizontal dimension, the thermal boundary condition, the lithosphere stratification and the strength of the crustal-mantle system, in agreement with previous parametric works (e.g. Marotta *et al.*, 1999; Gerya *et al.*, 2004). In particular the preliminary model T_1 predicts a rather long time span of ≈100 Ma from the collision onset to the unrooting, due to the limited horizontal extension of the model, which does not allow the development of an effective global convective flow and to the global low thermal regime, controlled by the assumed thermal boundary conditions. In model T_2, the unrooting process accelerates (time span of ≈40 Ma) as a

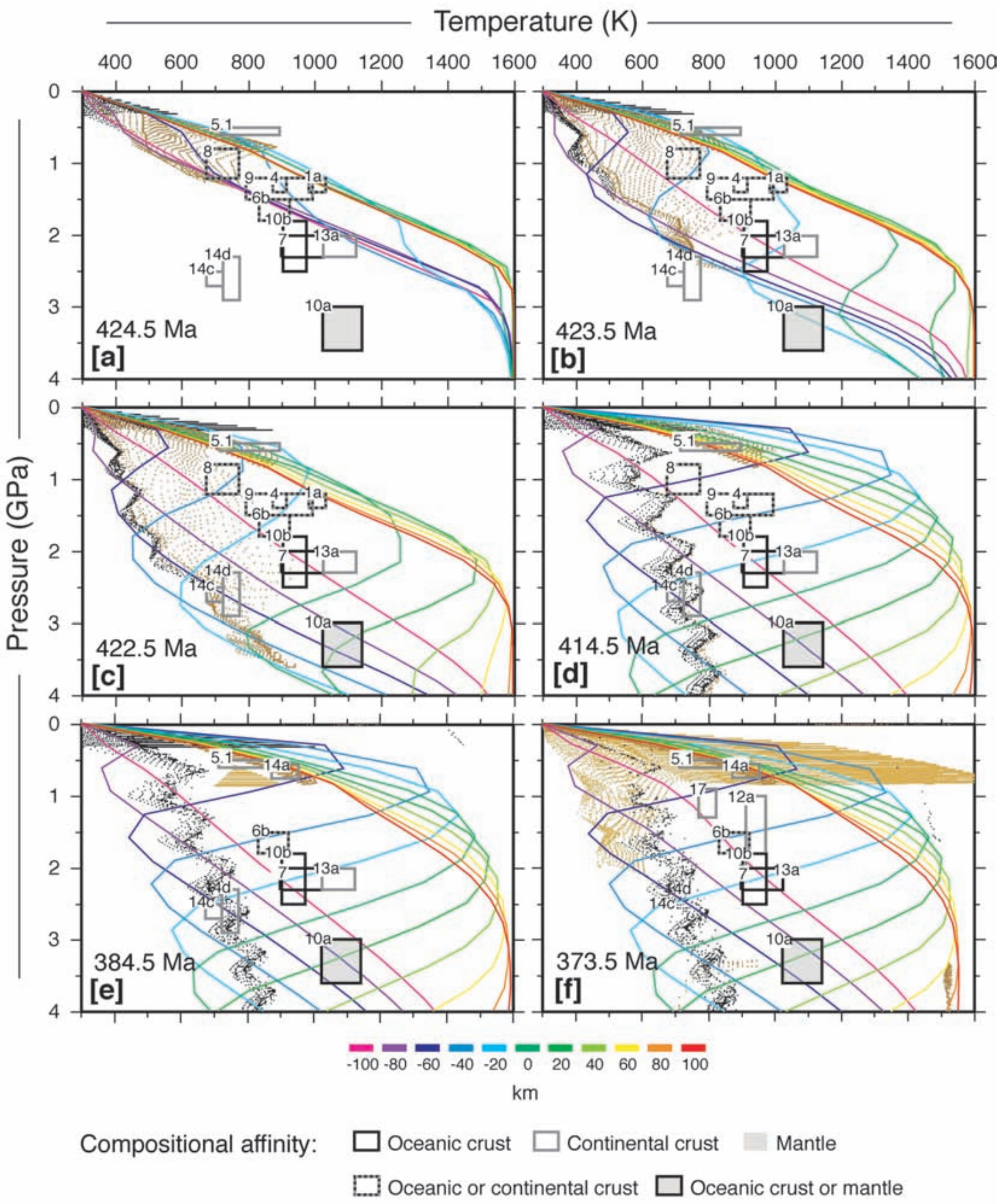

Fig. 17 – Variation in time of the vertical thermal profiles (a-f) at different distances from the suture zone (coloured lines and colour bar) during the active oceanic subduction phase, compared with P-T estimates inferred from rocks of oceanic or continental crust and mantle affinity, during the subduction phase (rectangles as listed in Table 1; keys in the legend). Black and ochre points indicate oceanic and continental crust markers, respectively, as described in the text. Ages indicated on each panel are absolute.

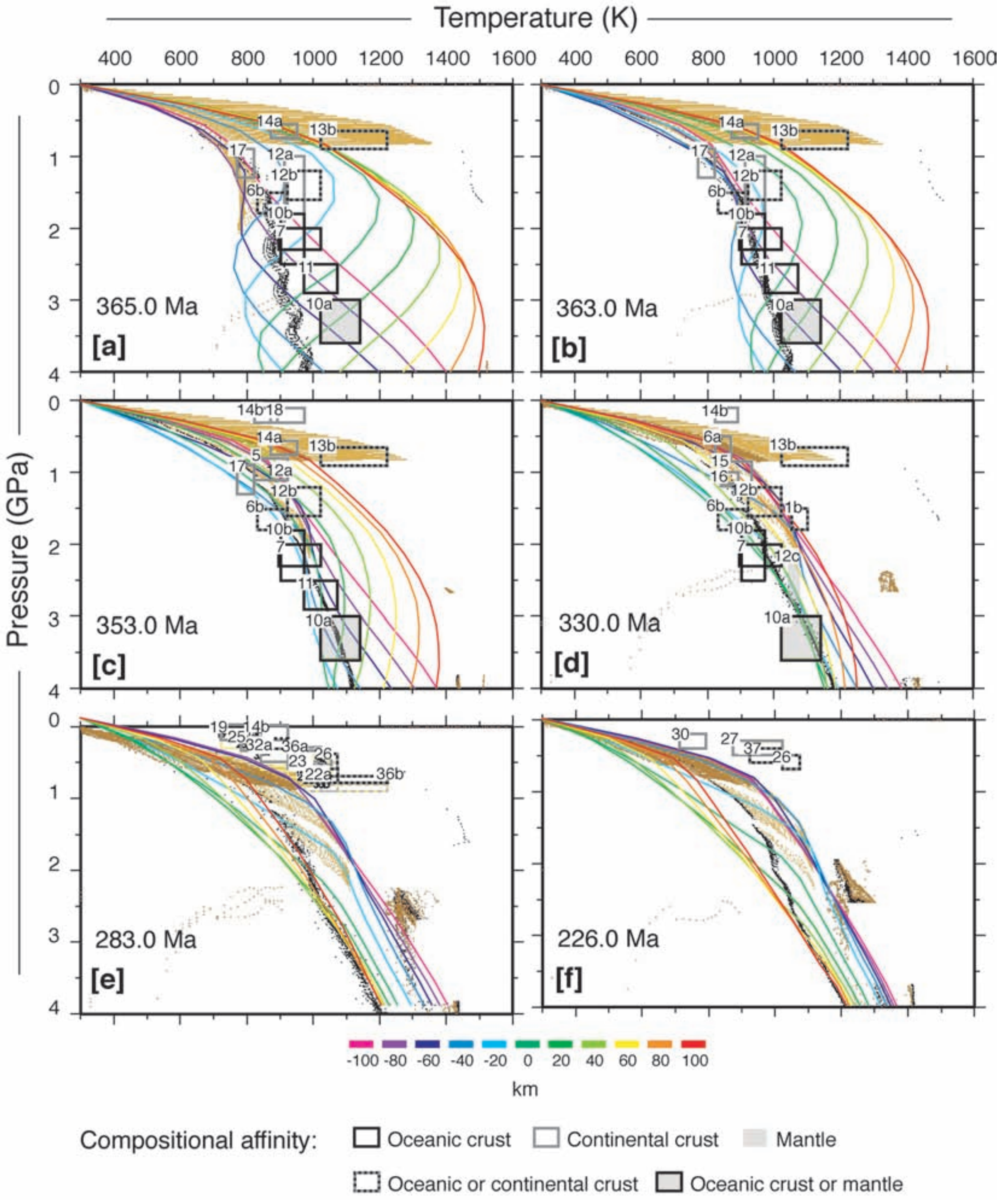

Fig. 18 – Variation in time of the vertical thermal profiles (a - f) at different distance from the suture zone (colored lines and palet) for the syn- to post-collision phase, compared with P-T estimates inferred from rocks of oceanic or continental crust and mantle affinity, during the Permian-Triassic age (rectangles as listed in Table 2; keys in the legend). Black and ochre points indicate oceanic and continental crust markers, respectively, as described in the text. Ages indicated on each panel are absolute.

consequence of a horizontally wider system and a higher thermal state. The very short span of time (≈7 Ma) characterising the unrooting process in model T_3 is consequent to the more realistic crust-mantle stratification, which makes the whole system rheologically softer.

Surface deformation configuration is characterized, for all the models, by alternating horizontal shortening and extension domains, with horizontal extension areas localising, for models T_2 and T_3, above the regions of subducted continental and oceanic lithosphere upwelling.

Concerning the comparison between natural and predicted P-T data, the most promising agreement, consisting of the coincidence of age, thermal gradient and compositional affinity (oceanic or continental crust, lithospheric mantle) is obtained with model T_3, even if it does not succeed to keep the fit, at least thermal, during Permian-Triassic period if a purely gravitational evolution is envisaged, in agreement with previous interpretations of the Permian-Triassic metamorphic evolution of Southalpine or Austroalpine tectonic units (e.g. Lardeaux and Spalla, 1991; Diella *et al.*, 1992). As detailed in Marotta and Spalla (2007), a forced extension is required to reproduce the thermal state appropriate to satisfy the fit with the natural data.

ACKNOWLEDGMENTS

M.I.S. is grateful to Ezio Callegari to have demonstrated to all his students the fundamental role of accurate petrography when exploiting the rock memory of past geologic history, which may be very extended in many Alpine tectonic units. Authors thank G. Gosso and R. Sabadini for fruitful discussion, D. Castelli for his thorough and accurate editorial work and the reviewers P. Allemand and M. Scambelluri for the constructive criticisms that improved the manuscript. M. I. Spalla was funded by the Italian Ministry of Universities and Research (M.I.U.R.) under a project entitled 'Structural markers of divergent and convergent tectonics in the crustal infrastructure of the Central-Western Alps' (COFIN 2005). A. M. Marotta was funded by the Italian Ministry of Universities and Research (M.I.U.R.) under a project entitled 'Strain and Stress analysis in the Central European Basin System: integration of numerical modelling with geological, geophysical and satellite data' (COFIN 2005). Figures 6, 7, 9-18 were created using GMT plotting software (Wessel and Smith, 1998).

REFERENCES

BARD J.P., BURG J.P., MATTE P. and RIBEIRO A. (1980) - *La chaine hercynienne d'Europe occidentale en terme de tectonique des plaques.* Colloque C6 du 26eme Congrés Géologique International, Paris, 233-246.

BEARDSMORE G.R. and CULL J.P. (2001) - *Crustal heat flow.* Cambridge Univ. Press, London, 324 pp.

BENCIOLINI L., POLI M.E., VISONÀ D. and ZANFERRARI A. (2006) - *Looking inside Late Variscan tectonics: structural and metamorphic heterogeneity of the Eastern Southalpine Basement (NE Italy).* Geodin. Acta, **19**, 17-32.

BERTOTTI G., SILETTO G.B. and SPALLA M.I. (1993) - *Deformation and metamorphism associated with crustal rifting: Permian to Liassic evolution of the Lake Lugano-Lake Como area (Southern Alps).* Tectonophysics, **226**, 271-284.

BEST M.G. and CHRISTIANSEN E.H. (2001) - *Igneous Petrology.* Blackwell Science, London, 458 pp.

BIAGINI L., BISTACCHI A., GOSSO G., MAGISTRONI C., ROSSETTI I., SPALLA M.I. and TOGNONI A. (1995) - *The II DK, HT mega-relic in the Sesia-Lanzo Zone, Late Variscan collision or Permo-Triassic rifting?* International Ophiolite Symposium, Pavia, 22.

BOCQUET J., DELALOYE M., HUNZIKER J.C. and KRUMMENACHER D. (1974) - *K-Ar and Rb-Sr dating of blue amphiboles, micas and associated minerals from the Western Alps.* Contrib. Mineral. Petrol., **47**, 7-26.

BOGDANOFF S., MENOT R. and VIVIER G. (1991) - *Les massif cristallins externes des Alpes occidentales francaises, un fragment de la zone interne Varisque.* Sci. Géol. Bull., **44**, 237-285.

BONIN B., BRAENDLEIN P., BUSSY F., DESMONS J., EGGENBERGER U., FINGER F., GRAF K., MARRO C., MERCOLLI I., OBERHAENSLI R., PLOQUIN A., VON QUADT A., VON RAUMER J., SCHALTEGGER U., STEYER HP., VISONÀ D. and VIVIER G. (1993) - *Late Variscan magmatic evolution of the Alpine basement.* In: Von Raumer J. and Neubauer F. (Eds.), Pre-Mesozoic geology in the Alps. Springer-Verlag, Berlin, 171-201.

BORGHI A., GATTIGLIO M., MONDINO F. and ZACCONE G. (1999) - *Structural and metamorphic evidence of pre-Alpine basement in the Ambin nappe (Cottian Alps, Italy).* Mem. Sci. Geol., **51**, 205-220.

BORIANI A. and BURLINI L. (1995) - *Carta Geologica della valle Cannobina Scala 1:25000.* Dip. Sci. Terra, Univ. Milano.

BORIANI A., COLOMBO A. and MACERA P. (1985) - *Radiometric geochronology of Central Alps.* Rend.

Soc. It. Mineral. Petrol., **40**, 139-186.

Boriani A. and Villa I.M. (1997) - *Geochronology of regional metamorphism in the Ivrea-Verbano Zone and Serie dei Laghi, Italian Alps.* Schweiz. Mineral. Petrogr. Mitt., **77**, 381-401.

Borsi S., Del Moro A., Sassi F.P., Visonà D. and Zirpoli G. (1980) - *On the existence of Hercynian aplites and pegmatites in the lower Aurina valley (Ahrntal, Austrides, Eastern Alps).* N. Jb. Miner. Mh., **1980**, 501-514.

Borsi S., Ferrara G., Paganelli L. and Simboli G. (1968) - *Isotopic age measurements of M. Monzoni intrusive complex*. Mineral. Petrogr. Acta, **14**, 171-183.

Bouffette J. (1993) - *Evolution tectonométamorphique des unites oceaniques et continentales au Nord du massif Dora-Maira (Alpes Occidentales).* PhD Thesis, Univ. Claude Bernard Lyon I, 230 pp.

Bouffette J., Lardeaux J.M. and Caron J.M. (1993) - *Le passage des granulites aux éclogites dans les métapélites de l'unité de la Punta Muret (Massif Dora-Maira, Alpes occidentales).* C. R. Acad. Sci., **317**, 1617-1624.

Boutin R., Montigny R. and Thuizat R. (1995) - *Chronologie K-Ar et Ar39/Ar40 du metamorphisme et du magmatisme des Vosges. Comparaison avec les massifs varisques avoisinant.* Géol. France, **1**, 3-25.

Brack P. (1981) - *Structures in the southwestern border of the Adamello intrusion (Alpi Bresciane).* Schweiz. Mineral. Petrogr. Mitt., **61**, 37-50.

Brodie K.H., Rex D. and Rutter E.H. (1989) - *On the age of deep crustal extensional faulting in the Ivrea zone, Northern Italy.* Geol. Soc. Lond. Spec. Pub., **45**, 203-210.

Brugger J. (1994) - *Les veines à andalousite du Pischahorn (Grisons, Suisse)*. Schweiz. Mineral. Petrogr. Mitt., **74**, 191-202.

Bussy F., Sartori M. and Thelin P. (1996) - *U-Pb zircon dating in the middle Penninic basement of the Western Alps (Valais, Switzerland).* Schweiz. Mineral. Petrogr. Mitt., **76**, 81-84.

Bussy F., Venturini C., Hunziker J. and Martinotti G. (1998) - *U-Pb ages of magmatic rocks of the Western Austroalpine Dent Blanche-Sesia Unit*. Schweiz. Mineral. Petrogr. Mitt., **78**, 163-168.

Cassinis R. (2006) - *Reviewing pre-TRANSALP DFF models.* Tectonophysics, **414**, 79-86.

Chopra P.N. and Peterson M.S. (1981) - *The experimental deformation of dunite.* Tectonophysics, **78**, 453-473.

Christensen U.R. (1992) - *An Eulerian Tecnique for thermo-mecahnical model of lithospheric extension.* J. Geophys. Res., **97**, 2015-2036.

Colombo A. and Tunesi A. (1999) - *Pre-Alpine metamorphism of the southern Alps.* Schweiz. Mineral. Petrogr. Mitt., **79**, 63-77.

Colombo F., Compagnoni R. and Lombardo B. (1994) - *Le rocce eclogitiche dei Laghi del Frisson (Argentera sud-orientale, Alpi Marittime).* Atti Tic. Sci. Terra, **1 s. spec.**, 75-82.

Cortesogno L., Cassinis G., Dallagiovanna G., Gaggero L., Oggiano G., Ronchi A., Seno S., Vanossi M. (1998) - *The Variscan post-collisional volcanism in Late Carboniferous-Permian sequences of Ligurian Alps, Southern Alps and Sardinia (Italy), a synthesis.* Lithos, **45**, 305-328.

Dal Piaz G.V. (1993) - *Evolution of Austroalpine and Upper Penninic basement in the NorthWestern Alps from Variscan convergence to post-Variscan extension.* In: Von Raumer J. and Neubauer F. (Eds.), Pre-Mesozoic geology in the Alps. Springer-Verlag, Berlin, 327-344.

Dal Piaz G.V. (2001) - *Geology of the Monte Rosa massif, historical review and personal comments.* Schweiz. Mineral. Petrogr. Mitt., **81**, 275-303.

Dal Piaz G.V., Cortiana G., Del Moro A., Martin S., Pennacchioni G. and Tartarotti P. (2001) - *Tertiary age and paleostructural inferences of the eclogitic imprint in the Austroalpine outliers and Zermatt-Saas ophiolite, Western Alps.* Int. J. Earth Sci., **90**, 668-684.

Dal Piaz G.V., De Vecchi G. and Hunziker J.C. (1977) - *The Austroalpine layered gabbros of the Matterhorn and Mt. Collon-Dents de Bertol.* Schweiz. Mineral. Petrogr. Mitt., **57**, 59-88.

Dal Piaz G.V., Gosso G., Pennacchioni G. and Spalla M.I. (1993) - *Geology of eclogites and related rocks in the Alps.* In: Morten L. (Ed.), Italian eclogites and related rocks, Acc. Naz. Sci, **13**, 17-58.

Dal Piaz G.V., Lombardo B. and Gosso G. (1983) - *Metamorphic evolution of the Mt. Emilius klippe, Dent Blanche nappe, Western Alps*. Am. J. Sci., **283A**, 438-458.

Debon F. and Lemmet M. (1999) - *Evolution of Mg/Fe ratios in late Variscan plutonic rocks from the external Crystalline Massifs of the Alps (France, Italy, Switzerland).* J. Petrol., **40**, 1151-1185.

Del Moro A. and Visonà D. (1982) - *The epiplutonic Hercynian Complex of Bressanone (Brixen, Eastern Alps, Italy) Petrologic and radiometric data.* N. Jb. Miner. Abh., **145**, 66-85.

Desmons J. (1992) - *The Briancon basement (Pennine Western Alps): mineral composition and polymetamorphic evolution.* Schweiz. Mineral. Petrogr. Mitt., **72**, 37-55.

Desmons J., Compagnoni R., Cortesogno L., Frey M. and Gaggero L. (1999) - *Pre-Alpine metamorphism of the internal zone of the Western Alps.* Schweiz. Mineral. Petrogr. Mitt., **79**, 23-39.

Di Paola S. (2001) - *Eredità Litostratigrafica, strutturale e metamorfica paleozoica nel margine interno europeo (Grandes Rousses e Argentera), ristrutturato durante l'orogenesi alpina*. PhD Thesis, Univ. Milano-Univ. Claude Bernard Lyon, 360 pp.

Di Paola S. and Spalla M.I. (2000) - *Contrasting tectonic records in pre-Alpine metabasites of the Southern Alps (Lake Como, Italy).* J. Geodyn., **30**, 167-189.

Diella V., Spalla M.I. and Tunesi A. (1992) - *Contrasted thermo-mechanical evolutions in the Southalpine metamorphic basement of the Orobic Alps (Central Alps, Italy).* J. Metam. Geol., **10**, 203-219.

Droop G.T.R. (1983) - *Pre-Alpine eclogites in the Pennine Basement Complex of the Estern Alps.* J. Metam. Geol, **1**, 3-12.

Droop G.T.R., Lombardo B. and Pognante U. (1990) - *Formation and distribution of eclogite facies rocks in the Alps*. In: Carswell D.A. (Ed.), Eclogite facies rocks. Blackie and Son Ltd, London, 225-256.

Dubois J. and Diament M. (1997) - *Géophysique*. Masson, Paris, 205 pp.

Engi M., Scherrer N.C. and Burri T. (2001) - *Metamorphic evolution of Pelitic rocks of the Monte Rosa nappe: Constraints from petrology and single grain monazite age data.* Schweiz. Mineral. Petrogr. Mitt., **81**, 305-328.

England P.C. and Thompson A.B. (1984) - *Pressure-Temperature-Time paths of regional metamorphism I. Heat transfer during the evolution of regions of thickened continental crust*. J. Petrol., **25**, 894-928.

Faure M., Ledru P., Lardeaux J.M. and Matte P. (2004) - *Paleozoic orogenies in the French Massif Central a cross section from Bèziers to Lyon.* Field Trip Guide Book - 32nd IGC- Florence, **B22**, 3-48.

Faure M., Leloix C. and Roig J.Y. (1997) - *L'evolution polycyclique de la chaine hercynienne.* Bull. Soc. Géol. France, **168**, 695-705.

Ferrara G. and Innocenti F. (1974) - *Radiometric age evidences of a Triassic thermal event in the Southern Alps.* Geol. Rundch, **63**, 572-581.

Ferry J.M., Wing B.A., Penniston-Dorland S.C. and Rumble D. (2002) - *The direction of fluid flow during contact metamorphism of siliceous carbonate rocks: new data for the Monzoni and Predazzo aureoles, northern Italy, and a global review.* Contrib. Mineral. Petrol., **142**, 679-699.

Finger F. and Quadt A. (1995) - *U-Pb ages of zircons from a plagiogranite-gneiss in the southeastern Bohemian massif, Austria: further evidence for an important early Paleozoic rifting episode in the eastern Variscides.* Schweiz. Mineral. Petrogr. Mitt., **75**, 265-270.

Gaidies F., Abart R., De Capitani C., Schuster R., Connolly J.A.D. and Reusser E. (2006) - *Characterization of polymetamorphism in the Austroalpine basement east of the Tauern Window using garnet isopleth thermobarometry.* J. Metam. Geol., **24**, 451-475.

Gardien V., Reusser E. and Marquer D. (1994) - *Pre-Alpine metamorphic evolution of the gneisses from the Valpelline Series (Western Alps, Italy).* Schweiz. Mineral. Petrogr. Mitt., **74**, 489-502.

Gebauer D. and Soellner F. (1993) - *U-Pb dating of zircons from eclogites of the Austroalpine Oetztal crystalline complex (E-Alps, Austria): conventional and SHRIMP data*. Terra Nova Abstr. Suppl., **4**, 10.

Gerya T.V. and Stoeckhert B. (2006) - *Two-dimensional numerical modeling of tectonic and metamorphic histories at active continental margins.* Int. J. Earth Sci., **95**, 250-274.

Gerya T.V., Yuen D.A. and Maresch W.V. (2004) - *Thermo-mechanical modelling of slab detatchment.* Earth Planet. Sci. Lett., **226**, 101-116.

Giacomini F., Messiga B., Tribuzio R. and Braga R. (1999) - *The Sondalo gabbroic complex and its country rocks: new geological and petrological data.* Tuebingen Geowiss. Arb., **A 52**, 156.

Giobbi Origoni E. and Gregnanin A. (1983) - *The crystalline basement of the "Massiccio delle tre Valli Bresciane": new petrographic and chemical data.* Mem. Soc. Geol. It., **26**, 133-144.

Giorgis D., Thelin P., Stampfli G. and Bussy F. (1999) - *The Mont-Mort metapelites: Variscan metamorphism and geodynamic context (Brianconnais basement, Western Alps, Switzerland).* Schweiz. Mineral. Petrogr. Mitt., **79**, 381-198.

Godard G., Martin S., Prosser G., Kienast J.R. and Morten L. (1996) - *Variscan migmatites, eclogites and garnet-peridotites of the Ulten zone, Eastern Austroalpine system.* Tectonophysiscs, **259**, 313-341.

Golonka J., Ross M.I. and Scotese C.R. (1994) - *Phanerozoic paleogeographic and paleoclimatic modeling maps.* Can. Soc. Petr. Geol., Memoir **17**, 1-47.

Gosso G., Messiga B. and Spalla M.I. (1995) - *Dumortierite-kyanite relics within the HT-LP country rocks of the Sondalo Gabbro: a record of* *extension related uplift of HP-rocks.* International Ophiolite Symposium, Pavia, 55.

Gregnanin A. (1980) - *Metamorphism and magmatism in the western italian Tyrol.* Rend. Soc. Ital. Miner. Petrol., **36**, 49-64.

Guillot S., Menot R. and Fernandez A. (1998) - *Paleozoic evolution of the external crystalline massifs along the Belledonne-Oisans transect (Western Alps).* Acta Univ. Carol. Geol., **42**, 257-259.

Haas R. (1985) - *Zur metamorphose des suedlichen Oetztalkristallins unter besonderer Beruecksichtigung der Matscher Einheit (Vintschgau/Suedtirol).* PhD Thesis, Innsbruck, 118 pp.

Habler G. and Thoeni M. (1998) - *Die praemesozoische Niederdruck-metamorphose in der polymetamorphen Gneisgruppe der NW Saualpe (Arbeitsgebiet N Knappenberg/Kaernten).* Mittt. Oesterr. Miner. Ges., **143**, 291-293.

Handy M.R. and Oberhaensli R. (2004) - *Explanatory notes to the map: Metamorphic structure of the Alps - Age map of metamorphic structure of the Alps - Tectonic interpretation and outstanding problems.* Mitt. Oesterr. Miner. Ges., **149**, 201-218.

Handy M.R. and Zingg A. (1991) - *The tectonic and rheological evolution of an attenuated cross-section of the continental crust: Ivrea crustal section, Southern Alps, Northwestern Italy and Southern Switzerland.* Geol. Soc. Am. Bull., **103**, 236-253.

Hansmann W., Muentener O. and Hermann J. (2001) - *U-Pb zircon geochronology of a tholeiitic intrusion and associated migmatites at a continental crust-mantle transition, Val Malenco, Italy.* Schweiz. Mineral. Petrogr. Mitt., **81**, 239-255.

Hauzenberger C., Hoeller W., Hoinkes G., Kloezli U. and Thoeni M. (1993) - *Metamorphic evolution of the Austroalpine basement in Nonsberg area, Ultental (Val d'Ultimo), Southern Tyrol.* Terra Nova, **5**, 13.

Henk A., Franz L., Teufel S. and Oncken O. (1997) - *Magmatic underplating, extension and crustal reequilibration: insights from a cross-section through the Ivrea zone and Strona Ceneri Zone, Northern Italy.* J. Geol., **105**, 367-377.

Hermann J. and Rubatto D. (2003) - *Relating zircon and monazite domains to garnet growth zones: age and duration of granulite facies metamorphism in the Val Malenco lower crust.* J. Metam. Geol., **21**, 833-852.

Herzberg C., Riccio L., Chiesa A., Fornoni A., Gatto G.O., Gregnanin A., Piccirillo E.M. and Scolari A. (1977) - *Petrogenetic evolution of a spinel-garnet-lherzolite in the Austridic crystalline basement from Val Clapa (Alto Adige, Northeastern Italy).* Mem. Sci. Geol., **30**, 1-28.

Hinterlechner-Ravnik A., Sassi F.P. and Visonà D. (1991a) - *The Austridic eclogites, metabasites and metaultrabasites from the Pohorje area (Easteen Alps, Yugoslavia); I: The eclogites and related rocks.* Rend. Fis. Acc. Lincei, **9**, 157-173.

Hinterlechner-Ravnik A., Sassi F.P. and Visonà D. (1991b) - *The Austridic eclogites, metabasites and metaultrabasites from the Pohorje area (Easteen Alps, Yugoslavia); 2: The metabites and metaultrabasites and concluding considerations.* Rend. Fis. Acc. Lincei, **9**, 175-190.

Hoke L. (1990) - *The Altkristallin of the Kreuzeck Mountains, SE-Tauern Window, Eastern Alps - basement crust in a convergent plate boundary zone.* Jb. Geol. B.-A., **133**, 5-87.

Holdaway M.J. (1971) - *Stability of andalusite and the aluminium silicate phase diagram.* Am. J. Sci., **271**, 97-131.

Hunziker J.C., Desmons J. and Hurford A.J. (1992) - *Thirty-two years of geochronological work in the Central and Western Alps: a review on seven maps.* Mém. Géol. Lausanne, **13**, 1-59.

Hunziker J.C. and Zingg A. (1980) - *Lower Paleozoic amphibolite to granulite facies metamorphism in the Ivrea Zone (southern Alps, northern Italy).* Schweiz. Miner. Petrogr. Mitt., **60**, 181-213.

Janak M., Vrabec M., Horvath P., Konecny P. and Luptak B. (2003) - *High-pressure to ultrahigh-pressure metamorphism of kyanite eclogites from Pohorje, Slovenia: microtextural and thermobarometric evidence.* Geophys. Res. Abstr., **5**, 08468.

Kirby S.H. (1983) - *Rheology of the litosphere.* Rev. Geophys. Space Phys., **21**, 1458-1487.

Konzett J., Miller C., Armstrong R. and Thoeni M. (2005) - *Metamorhic evolution of Iron-rich Mafic cumulates from the Oetztal-Stubai Crystalline Complex, Eastern Alps, Austria.* J. Petrol., **46**, 717-747.

Kretz R. (1983) - *Symbols for rock-forming minerals.* Am. Mineral., **68**, 277-279.

Lardeaux J.M. (1981) - *Evolution tectono-metamorphique de la zone nord du Massif de Sesia-Lanzo (Alpes occidentales): un exemple d'éclogitisation de croute continentale.* PhD Thesis, Paris VI, 226 pp.

Lardeaux J.M. and Spalla M.I. (1990) - *Tectonic significance of P-T-t paths in metamorphic rocks: examples from ancient and modern orogenic belts.* Mem. Soc. Geol. It., **45**, 51-69.

Lardeaux J.M. and Spalla M.I. (1991) - *From granulites to eclogites in the Sesia zone (Italian Western Alps): a record of the opening and closure of the Piedmont ocean.* J. Metam. Geol., **9**, 35-59.

Latouche L. and Bogdanoff S. (1987) - *Evolution précoce du massif de l'Argentera: apport des eclogites et des granulites.* Géol. Alp., **63**, 151-164.

Le Bayon B., Pitra P., Ballevre M. and Bohn M. (2006) - *Reconstructing P-T paths during continental collision using multi-stage garnet (Gran Paradiso nappe, Western Alps).* J. Metam. Geol., **24**, 477-496.

Ledru P., Courrioux G., Dallain C., Lardeaux J.M., Montel J.M., Vanderhaeghe O. and Vitel G. (2001) - *The Velay dome (French Massif Central): melt generation and granite emplacement during orogenic evolution.* Tectonophysics, **332**, 207-237.

Ledru P., Lardeaux J.M., Santallier D., Autran A., Quenardel J.M., Floc'h J.P., Lerouge G., Maillet N., Marchand J. and Ploquin A. (1989) - *Où sont les nappes dans le Massif Central français?* Bull. Soc. Géol. Fr., **8**, 605-618.

Liegeois J.-P. and Duchesne J.-C. (1981) - *The Lac Cornu retrograded eclogites (Aiguilles Rouges massif, Western Alps, France): evidence of crustal origin and metasomatic alteration.* Lithos, **14**, 35-48.

Lombardo B., Colombo F., Compagnoni R., Ghiglione G. and Rubatto D. (1997) - *Relics of pre-Variscan events in the Malinvern-Argentera Complex, Argentera Massif, Western Alps.* Quad. Geod. Alp. Quat., **4**, 66.

Lu M., Hoffmann A.W., Mazzucchelli M. and Rivalenti G. (1997) - *The mafic-ultramafic complex near Finero (Ivrea-Verbano Zone): II. Geochronology and isotope geochemistry.* Chem. Geol., **140**, 223-235.

Maggetti M. and Flisch M. (1993) - *Evolution of the Silvretta nappe.* In: von Raumer J.F. and Neubauer F. (Eds.), Pre-Mesozoic geology in the Alps. Springer-Verlag, Berlin, 469-484.

Maggetti M. and Galetti G. (1988) - *Evolution of the Silvretta eclogites: metamorphic and magmatic events.* Schweiz. Miner. Petrog. Mitt., **68**, 467-484.

Malavieille J. (1993) - *Late orogenic extension in mountain belts: insights from the Basin and Range and the Late Paleozoic Variscan Belt.* Tectonics, **12**, 1115-1130.

Malavieille J., Guihot P., Costa S., Lardeaux J.M. and Gardien V. (1990) - *Collapse of the thickened Variscan crust in the French Massif Central: Mont Pilat extensional shear zone and St. Etienne Late Carboniferous basin.* Tectonophysics, **177**, 139-149.

Marotta A.M., Fernandez M. and Sabadini R. (1999) - *Mantle unrooting in collisional settings.* Tectonophysics, **296**, 31-46.

Marotta A.M. and Spalla M.I. (2007) - *Permian-Triassic high thermal regime in the Alps: result of Late Variscan collapse or continental rifting? Validation by numerical modeling.* Tectonics, DOI 10.1029/2006TC002047.

Marotta A.M., Spelta E. and Rizzetto C. (2006) - *Gravity signature of crustal subduction inferred from numerical modelling.* Geophys. J. Int., **166**, 923-938.

Matte P. (1986) - *Tectonics and plate tectonics model for the Variscan belt of Europe.* Tectonophysics, **126**, 329-374.

Mayer A., Mezger K. and Sinigoi S. (2000) - *New Sm-Nd ages for the Ivrea-Verbano Zone, Sesia and Sessera valleys (Northern Italy).* J. Geodyn., **30**, 147-166.

Melcher F., Meisel T., Puhl J. and Koller F. (2002) - *Petrogenesis and geotectonic setting of ultramafic rocks in the Eastern Alps: constraints from geochemistry.* Lithos, **65**, 69-112.

Menot R.P. and Paquette J.L. (1993) - *Geodynamic significance of basic and bimodal magmatism in the external domain.* In: von Raumer J.F. and Neubauer F. (Eds.), Pre-Mesozoic geology in the Alps. Springer-Verlag, Berlin, 241-254.

Messiga B., Tribuzio R. and Caucia F. (1992) - *Amphibole evolution in Variscan eclogite-amphibolites of the Savona crystalline massif (Western Ligurian Alps, Italy): controls on the decompressional P-T-t path.* Lithos, **27**, 215-230.

Milano P.F., Pennacchioni G. and Spalla M.I. (1988) - *Alpine and pre-Alpine tectonics in the Central Orobic Alps (Southern Alps).* Eclogae Geol. Helv., **81**, 273-293.

Miller C. and Thoeni M. (1995) - *Origin of eclogites from the Austroalpine Oetztal basement (Tirol, Austria): geochemistry and Sm-Nd vs Rb-Sr isotope systematics.* Chem. Geol., **122**, 199-225.

Miller C. and Thoeni M. (1997) - *Eo-Alpine eclogitisation of Permian MORB-type gabbros in the Koralpe (Eastern Alps, Austria): new geochronological, geochemical and petrological data.* Chem. Geol., **137**, 283-310.

Monie P. (1990) - *Preservation of Hercynian 40Ar/39Ar ages through high-pressure low-temperature Alpine metamorphism in the Western Alps.* Eur. J. Mineral., **2**, 343-361.

Monjoie P., Bussy F., Lapierre H. and Pfeifer H.R.

(2005) - *Modeling of in-situ crystallization processes in the Permian mafic layered intrusion of Mont Collon (Dent Blanche nappe, Western Alps).* Lithos, **83**, 317-346.

Monjoie P., Bussy F., Lapierre H., Pfeifer H.R. and Bosch D. (2004) - *The Mont Collon mafic complex (Austroalpine Dent Blanche nappe) Permina evolution of the Western European mantle.* In: S.G.d.F.-G. Vereinigung, Joint Earth Sciences Meeting, 2004 - Strasbourg, RSTGV-A-00308.

Morten L., Nimis P. and Rampone E. (2004) - *Records of mantle-crust exchange processes during continental subduction-exhumation in the Nonsberg-Ultental garnet peridotites (Eastern Alps). A review.* Per. Mineral., **73**, 119-129.

Muentener O., Hermann J. and Trommsdorff V. (2000) - *Cooling history and exhumation of lower crustal granulite and upper mantle (Malenco, Eastern Central Alps).* J. Petrol., **41**, 175-200.

Mundil R., Brack P. and Laurenzi M.A. (1996) - *High resolution U-Pb single-zircon age determinations: new constraints on the timing of Middle Triassic magmatism in the Southern Alps. Geologia delle Dolomiti.* Soc. Geol. It., 78ª Riunione Estiva.

Muttoni G., Kent D.V., Garzanti E., Brack P., Abrahamsen N. and Gaetani M. (2003) - *Early Permian Pangea "B" to Late Permian Pangea "A".* Earth Planet. Sci. Lett., **215**, 379-394.

Neubauer F., Hoinkes G., Sassi F.P., Handler R., Hoeck V., Koller F. and Frank W. (1999) - *Pre-Alpine metamorphism of the Eastern Alps.* Schweiz. Mineral. Petrogr. Mitt., **79**, 41-62.

Nicot E. (1977) - *Les roches meso and catazonales de la Valpelline (nappe de la Dent Blanche; Alpes Italiennes).* Phd Thesis, Univ. Paris VI, Paris, 211 pp.

Nussbaum C., Marquer D. and Biino G.G. (1998) - *Two subduction events in a polycyclic basement: Alpine and pre-Alpine high-pressure metamorphism in the Suretta nappe, Swiss Eastern Alps.* J. Metam. Geol., **16**, 591-605.

Oliver G.J.H., Corfu F. and Krogh T.E. (1993) - *U-Pb ages from SW Poland: evidence for a Caledonian suture zone between Baltica and Gondwana.* J. Geol. Soc., London, **150**, 355-368.

Paquette J.L., Menot R. and Peucat J.J. (1989) - *REE, Sm-Nd and U-Pb zircon study of eclogites from the Alpine External Massifs (Western Alps): evidence for crustal contamination.* Earth Planet. Sci. Lett., **96**, 181-198.

Peacock S.M. (1989) - *Thermal modeling of metamorphic P-T-t paths.* Short course in Geology - Am. Geophys. Union, **7**, 57-102.

Pennacchioni G. and Cesare B. (1997) - *Ductile-brittle transition in pre-Alpine amphibolite facies mylonites during evolution from water-present to water-deficient conditions (Mont Mary nappe, Italian Western Alps).* J. Metam. Geol., **15**, 777-791.

Pfiffner A., Lehner P., Heitzman P.Z., Mueller S. and Steck A. (1997) - *Deep structure of the Swiss Alps - Results from NRP 20.* Birkhauser AG., Basel, 380 pp.

Pin C. (1986) - *Datation U-Pb sur zircon à 285 Ma du complexe gabbro dioritique du Val Sesia- Val Mastallone et âge tardi-hercynien du métamorphisme granulitique de la zone Ivrea-Verbano (Italie).* C.R. Acad. Sci. Paris, **303**, 827-830.

Pin C. (1990) - *Variscan oceans: ages, origins and geodynamic implications inferred from geochemical and radiometric data.* Tectonophysics, **177**, 215-227.

Pin C. and Peucat J.J. (1986) - *Ages des épisodes de metamorphisme paléozoique dans le Massif Central Française et le Massif Armoricain.* Bull. Soc. Géol. Fr., **8**, 461-469.

Platt J.P. (1986) - *Dynamics of orogenic wedges and the uplift of high-pressure metamorphic rocks.* Geol. Soc. Am. Bull., **97**, 1037-1053.

Platt J.P. (1993) - *Exhumation of high-pressure rocks: a review of concepts and processes.* Terra Nova, **5**, 119-133.

Polino R., Dal Piaz G.V. and Gosso G. (1990) - *Tectonic erosion at the Adria margin and accretionary processes for the Cretaceous orogeny of the Alps.* Mem. Soc. Géol. Fr., **N.S. 156**, 345-367.

Povoden, E., Horacek, M. and Abart, R. (2002) - *Contact metamorphism of siliceous dolomite and impure limestones from the Werfen formation in the eastern Monzoni contact aureole.* Mineral. Petrol., **76**, 99-120.

Quick J.E., Sinigoi S., Negrini L., Demarchi G. and Mayer A. (1992) - *Synmagmatic deformation in the underplated igneous complex of the Ivrea-Verbano zone.* Geology, **20**, 613-616.

Rahn M. (1991) - *Eclogites from the Minugrat, Siviez-Mischabel nappe (Valais, Switzerland).* Schweiz. Miner. Petrogr. Mitt., **71**, 415-426.

Rampone E. (2002) - *Mantle dynamics during Permo-Mesozoic extension of the Europe-Adria lithosphere: insights from the Ligurian ophiolites.* Per. Mineral., **73**, 215-230.

Ranalli G. and Murphy D.C. (1987) - *Rheological stratification of the lithosphere.* Tectonophysics, **132**, 281-295.

REBAY G. and SPALLA M.I. (2001) - *Emplacement at granulite facies conditions of the Sesia-Lanzo metagabbros: an early record of Permian rifting?* Lithos, **58**, 85-104.

RIKLIN K.A. (1983) - *Kontaktmetamorphose Permischer Sandsteine im Adamello Massif.* PhD thesis Thesis, Zürich, 140 pp.

ROTTURA A., BARGOSSI G.M., CAGGIANELLI A., DEL MORO A., VISONÀ D. and TRANNE C.A. (1998) - *Origin and significance of the Permian high-K calc-alkaline magmatism in the central-eastern Southern Alps, Italy.* Lithos, **45**, 329-348.

RUBATTO D., SCHALTEGGER U., LOMBARDO B., COLOMBO F. and COMPAGNONI R. (2001) - *Complex Paleozoic magmatic and metamorphic evolution in the Argentera Massif (Western Alps) resolved with U-Pb dating.* Schweiz. Mineral. Petrogr. Mitt., **81**, 213-228.

RYBACH L. (1988) - *Determination of heat production rate. Handbook of terrestrial heat-flow density determination.* Kluwer Academic Publishers, Dordrecht, 125-142.

SANDERS C.A.E., BERTOTTI G., TOMMASINI S., DAVIES G.R. and WIJBRANS J.R. (1996) - *Triassic pegmatites in the Mesozoic middle crust of the Southern Alps (Italy): fluid inclusions, radiometric dating and tectonic implications.* Eclogae Geol. Helv., **89**, 505-525.

SANDIFORD M. and POWELL R. (1986) - *Deep crustal metamorphism during crustal extension: modern and ancient examples.* Earth Planet. Sci. Lett., **79**, 151-158.

SASSI R., MAZZOLI C., MILLER C. and KONZETT J. (2004) - *Geochemistry and metamorphic evolution of the Pohorje Mountain eclogites from the easternmost Austroalpine basement of the eastern Alps (Northern Slovenia).* Lithos, **78**, 253-261.

SCHMID S. M., FUGENSCHUH B., KISSLING E. and SCHUSTER R. (2004) - *Tectonic map and overall architecture of the Alpine orogen*. Eclogae Geol. Helv., **97**, 93 – 117.

SCHUSTER R. and FRANK W. (2000) - *Metamorphic evolution of the Austroalpine units east of the Tauern Window: indications for Jurassic strike slip tectonics.* Mitt. Ges. Geol. Bergbaustud. Oesterr., **42**, 37-58.

SCHUSTER R., SCHARBERT S., ABART R. and FRANK W. (2001) - *Permo-Triassic extension and related HT/LP metamorphism in the Austroalpine-Southalpine realm.* Mitt. Ges. Geol. Bergbaustud. Oesterr., **45**, 111-141.

SCHWEINEHAGE R. and MASSONNE H.J. (1999) - *Geochemistry and metamorphic evolution of metabasites from the Silvretta nappe, Eastern Alps.* Mem. Sci. Geol., **51**, 191-203.

SILLS J.D. (1984) - *Granulite facies metamorphism in the Ivrea Zone, N.W. Italy.* Schweiz. Miner. Petrogr. Mitt., **64**, 169-191.

SPALLA M.I., CARMINATI E., CERIANI S., OLIVA A. and BATTAGLIA D. (1999) - *Influence of deformation partitioning and metamorphic re-equilibration on P-T path reconstruction in the pre-Alpine basement of central Southern Alps (Northern Italy).* J. Metam. Geol., **17**, 319-336.

SPALLA M.I., DIELLA V., PIGAZZINI N., SILETTO G.B. and GOSSO G. (2006) - *Significato tettonico della transizione Cld-And nelle metapeliti del Basamento Sudalpino (Alta Val Camonica).* Rend. Soc. Geol. It., **2**, 182-183.

SPALLA M.I. and GOSSO G. (1999) - *Pre-Alpine tectono-metamorphic units in the central Southern Alps: structural and metamorphic memory.* Mem. Sci. Geol., **51**, 221-229.

SPALLA M.I. and GOSSO G. (2003) - *Permian-Triassic magmatism and the tectonothermal evolution of the Austroalpine and South-Alpine lithosphere.* In: Transalp conference – Trieste 10-12 February 2003 - Mem. Sci. Geol., **54**, 105 – 108.

SPALLA M.I., LARDEAUX J.M., DAL PIAZ G.V., GOSSO G. and MESSIGA B. (1996) - *Tectonic significance of alpine eclogites.* J. Geodyn., **21**, 257-285.

SPALLA M.I., MESSIGA B. and GOSSO G. (1995) - *LT-alpine overprint on the HT-rifting related metamorphism in the steep belt of the Languard - Campo nappe. The Cima Rovaia and Scisti del Tonale units represent two different extents of alpine re-equilibration.* International Ophiolite Symposium, Pavia 1995, 148.

SPALLA M.I., ZANONI D., GOSSO G. and ZUCALI M. (2007) - *Deciphering the geologic memory of a Permian conglomerate of the Southern Alps by pebble P–T estimates.* Intern. J. Earth Sci., DOI 10.1007/s00531-007-0241-8.

SPALLA M.I., ZANONI D., SPREAFICO E., ZUCALI M. and GOSSO G. (2004) - *Metamorphic signature of crustal thinning in post-Variscan cover of central Southern Alps.* Joint Earth Sciences Meeting, Strasbourg, Abstract CD-ROM, RSTGV-A-00067.

SPEAR F.S. (1993) - *Metamorphic phase equilibria and Pressure-Temperature-time paths.* Min. Soc. Am. monograph., Washington, 799 pp.

STAEHLE V., FRENZEL G., KOBER B., MICHARD A., PUCHELT H. and SCHNEIDER W. (1990) - *Zircon syenite pegmatites in the Finero peridotite (Ivrea zone): evidence for a syenite from a mantle source.* Earth Planet. Sci. Lett., **101**, 196-205.

Staehle V., Frenzel G., Hess J.C., Saup F., Schmidt S.T. and Scneider W. (2001) - *Permian metabasalt and Triassic alkaline dykes in the northern Ivrea zone: clues to the post-Variscan geodynamic evolution of the Southern Alps.* Schweiz. Mineral. Petrogr. Mitt., **81**, 1-21.

Stoeckhert B. (1987) - *Das UttenheimerPegmatitfeld (Ostalpines Altkristallin, Suedtirol) Genese und alpine Ueberpraegung.* Erlanger Geol. Abh., **114**, 83-106.

Tait J.A., Bachtadse V., Franke W. and Soffel H.C. (1997) - *Geodynamic evolution of the European Variscan fold belt: paleomagnetic and geological constraints.* Geol. Rundch., **86**, 585-598.

Tao W.C. and O'Connel R.J. (1992) - *Ablative subduction: a two-sided alternative to the conventional subduction model.* J. Geophys. Res., **97**, 8877-8904.

Thelin P., Sartori M., Burri T., Gouffon Y. and Chessex R. (1993) - *The pre-Alpine basement of the Brianconnais (Wallis, Switzerland).* In: von Raumer J.F. and Neubauer F. (Eds.), Pre-Mesozoic Geology in the Alps. Springer-Verlag, Berlin, 297-315.

Thelin P., Sartori M., Lengeler R. and Scharer J.P. (1990) - *Eclogites of Paleozoic or Early-Alpine age in the basement of the Penninic Siviez-Mischabel nappe, Valais, Switzerland.* Lithos, **25**, 71-88.

Thoeni M. and Jagoutz E. (1992) - *Some new aspect of dating eclogites in orogenic belts: Sm-Nd, Rb-Sr, and Pb-Pb isotopic results from the Austroalpine Saualpe and Koralpe type-locality (Karinthia/Styria, southeastern Austria).* Geochim. Cosmochim. Acta, **56**, 347-368.

Thoeni M., Mottana A., Delitala M.C., De Capitani L. and Liborio G. (1992) - *The Val Biandino composite pluton: a Late Hercynian intrusion into the South Alpine metamorphic basement of the Alps (Italy).* N. Jb. Miner Mh., **12**, 545-554.

Thompson A.B. (1981) - *The Pressure-Temperature (P,T) plane viewed by geophysicists and petrologists.* Terra Cognita, **1**, 11-20.

Thompson A.B. and England P.C. (1984) - *Pressure-Temperature-Time paths of regional metamorphism II. Their inference and interpretation using mineral assemblages in metamorphic rocks.* J. Petrol., **25**, 929-955.

Torsvik, T.H. (1998) - *Palaeozoic palaeogeography: a North Atlantic viewpoint.* GFF, **120**, 109-118.

Tribuzio R., Thirlwall M.F. and Messiga B. (1999) - *Petrology, mineral and isotope geochemistry of the Sondalo gabbroic complex (Central Alps, Northern Italy): implications for the origin of post-Variscan magmatism.* Contrib. Mineral. Petrol., **136**, 48-62.

Tumiati S., Thoeni M., Nimis P., Martin S. and Mair V. (2003) - *Mantle-crust interactions during Variscan subduction in the Eastern Alps (Nonsberg-Ulten zone): geochronology and new petrological constraints.* Earth Planet. Sci. Lett., **210**, 509-526.

Turcotte D.L. and Schubert G. (2002) - *Geodynamics, 2nd edition.* Cambridge Univ. Press, 456 pp.

Vavra G., Gebauer D., Schmid R. and Compston W. (1996) - *Multiple zircon growth and recrystallization during polyphase Late Carboniferous to Triassic metamorphism in the Ivrea Zone (Southern Alps): an ion microprobe (SHRIMP) study.* Contrib. Mineral. Petrol., **122**, 337-358.

Vavra G., Schmid R. and Gebauer D. (1999) - *Internal morphology, habit and U-Th-Pb microanalysis of amphibolite- to -granulite facies zircons: geochronology of the Ivrea Zone (Southern Alps).* Contrib. Mineral. Petrol., **134**, 380-404.

Venturini G. (1995) - *Geology, Geochemistry and Geochronology of the inner central Sesia Zone (Western Alps - Italy).* Mém. Géol. Lausanne, **25**, 1-148.

Visonà D. (1995) - *Polybaric evolution of calc-alkaline magmas: the dioritic belt of the Bressanone-Chiusa igneous complex (NE Italy).* Mem. Sci. Geol., **47**, 111-124.

Visonà D. (1997) - *The Predazzo multipulse intrusive body (Western Dolomites, Italy). Field and mineralogical studies.* Mem. Sci. Geol., **49**, 117-125.

Vivier G., Menot R. and Giraud P. (1987) - *Magmatisme et structuration orogénique paleozoìque de la chaìne de Belledonne (massif cristallins externes alpins).* Géol. Alp., **63**, 25-53.

von Quadt A., Guenther D., Frischknecht R. and Franz G. (1997) - *The evolution of pre-Variscan eclogites of the Tauern Window (eastern Alps): A Sm/Nd conventional and Laser ICP-MS zirc0n U-Pb study.* Schweiz. Mineral. Petrogr. Mitt., **77**, 265-279.

von Raumer J.F. and Neubauer F. (1993) - *Pre-Mesozoic Geology in the Alps*. Springer-Verlag, Berlin, 677 pp.

von Raumer J., Stampfli G., Borel G. and Bussy F. (2002) - *Organization of pre-Variscan basement areas at the north-Gondwanan margin.* Int. J. Earth Sci., **91**, 35-52.

von Raumer J., Stampfli G. and Bussy F. (2003) - *Gondwana-derived microcontinents - the constituents of the Variscan and Alpine collisional orogen.* Tectonophysics, **365**, 7-22.

von Raumer J.F. (1974) - *Zur Metamorphose amphibolitischer Gesteine im Altkristallin des*

Mont-Blanc- und Aguilles -Rouges Massdaivs. Schweiz. Mineral. Petrogr. Mitt., **54**, 471-488.

von Raumer J.F., Abrecht J., Bussy F., Lombardo B., Menot R. and Schaltegger U. (1999) - *The Paleozoic metamorphic evolution of the Alpine External Massif.* Schweiz. Mineral. Petrogr. Mitt., **79**, 5-22.

Voshage H., Hunziker J.C., Hoffmann A.W. and Zingg A. (1987) - *A Nd and Sr isotopic study of Ivrea zone, Southern Alps, N-Italy*. Contrib. Mineral. Petrol., **97**, 31-42.

Vuichard J.P. (1987) - *Conditions P-T du métamorphisme antéalpin dans la "seconde zone diorito-kinzigitique" (Zone Sesia-Lanzo, Alpes occidentales).* Schweiz. Mineral. Petrogr. Mitt., **67**, 257-271.

Wessel P. and Smith W. H. F. (1998) - *New improved version of the Generic Mapping Tools released.* Eos Trans. AGU, **79**, 579.

Wopfner H. (1984) - *Permian deposits of the Southern Alps as product of initial Alpidic taphrogenesis.* Geol. Rundch., **73**, 259-277.

Ziegler P.A. (1986) - Geodynamic model for the Paleozoic crustal consolidation of Western and Central Europe. Tectonophysics, **126**, 303-328.

Ziegler P.A. (1993) - *Late Palaeozoic-Early Mesozoic plate reorganization: evolution and demise of the Variscan fold belt.* In: Von Raumer J.F. and Neubauer F. (Eds.), Pre-Mesozoic geology in the Alps. Springer-Verlag, Berlin, 203-216.

Zimmerman R. and Franz G. (1989) - *Die Eklogite der Unteren Schieferhuelle: Frosniztal/Suedvenediger (Tauern, Oesterreich).* Mitt. Oesterr. Geol. Ges., **81**, 167-188.

Zucali M. (2001) - *La correlazione nei terreni metamorfici: due esempi dall'Austroalpino occidentale (Zona Sesia-Lanzo) e centrale (Falda Languard-Campo/Serie del Tonale)*. PhD Thesis, Univ. Milano, 223 pp